The annual salinity cycle of the Denmark Strait Overflow

J.G. Opher[1,2,3,4], J.A. Brearley[1], S.R. Dye[2,3], R.S. Pickart[5], I.A. Renfrew[2], B.E. Harden[6], M.P. Meredith[1]

[1]British Antarctic Survey, High Cross, Madingley Road, Cambridge, UK, CB3 0ET

[2]School of Environmental Sciences, University of East Anglia, Norwich, UK, NR4 7TJ

[3]Centre for Environment, Fisheries and Aquaculture Science, Pakefield Road, Lowestoft, UK, NR33 0HT

[4]Now at Ocean Environment Team, UK Hydrographic Office, Taunton, UK

[5] Woods Hole Oceanographic Institution, Woods Hole, Massachusetts, USA, MA 02543

[6]Sea Education Association, Woods Hole, Massachusetts, USA, MA 02543

Corresponding author: Jacob Opher (jakeopher@hotmail.com)

Key Points:

- We identify an annual salinity cycle in the Denmark Strait Overflow of 0.02 peak to trough amplitude, with a minimum in May
- Freshening of the low salinity lid of the overflow at Denmark Strait in spring likely contributes to the freshening
- Salinity anomalies advect from the Shelfbreak East Greenland Current north of Denmark Strait to the overflow in the Irminger Basin

Abstract

The Denmark Strait Overflow (DSO) is an important source of dense water input to the deep limb of the Atlantic Meridional Overturning Circulation. It is fed by separate currents from the north that advect dense water masses formed in the Nordic Seas and Arctic Ocean which then converge at Denmark Strait. Here we identify an annual salinity cycle of the DSO, characterized by freshening in winter and spring. The freshening is linked to freshening of the Shelfbreak East Greenland Current in the Blosseville Basin north of the Denmark Strait. We demonstrate that the East Greenland Current advects fresh pycnocline water above the recirculating Atlantic Water, which forms a low salinity lid for the overflow in Denmark Strait and in the Irminger Basin. This concept is supported by intensified freshening of the DSO in lighter density classes on the Greenland side of the overflow. The salinity of the DSO in the Irminger Basin is significantly correlated with northerly/northeasterly winds in the Blosseville Basin at a lag of 3-4 months, consistent with estimated transit times. This suggests that wind driven variability of DSO source water exerts an important influence on the salinity variability of the downstream DSO, and hence the composition of the deep limb of the Atlantic Meridional Overturning Circulation.

Plain Language Summary

The warm surface waters of the Gulf Stream that flow northwards towards the Arctic are balanced by cold water flowing at depth in the other direction. The densest of these cold currents is the Denmark Strait Overflow, which flows across the sill between Greenland and Iceland before rapidly descending in the Atlantic Ocean. We analyzed the seasonal salinity variability of this overflow using ocean measurements at intervals along its pathway. Our analysis reveals an annual cycle in the salinity of the overflow for the first time, which is not detected in ocean records previously used to monitor the overflow. The seasonality is caused by winds blowing over a surface current which feeds the overflow – the East Greenland Current. Our study highlights the important role of wind in controlling overflow salinity variability and emphasizes that there are multiple distinct sources that contribute to the overflow salinity.

1 Introduction

The Denmark Strait Overflow (DSO) advects dense water southward and makes an important contribution to the deep limb of the Atlantic Meridional Overturning Circulation (AMOC). The time mean volume transport of the DSO through Denmark Strait (DS), between Iceland and Greenland, is estimated to be between 3.2–3.5 Sv (1 Sv = 10^6 m^3 s^{-1}) (Harden et al., 2016; Jochumsen et al., 2017), which increases to around 5 Sv downstream in the Irminger Basin, after entrainment of warm ambient water (Dickson & Brown, 1994).

The dense source water for the DSO is advected from the north, via three main current branches – the Shelfbreak East Greenland Current (EGC), the Separated EGC and the North Icelandic Jet (NIJ) (Våge et al., 2013) (Figure 1). The EGC originates in Fram Strait and flows southward along the shelfbreak before bifurcating at around 69°N, with one branch continuing along the shelfbreak (the Shelfbreak EGC) and the other separating from the bathymetry and flowing southward towards the Iceland slope (the Separated EGC). The NIJ emerges on the continental slope north of Iceland and flows towards the DS on the mid-Iceland slope (Semper et al., 2019) (Figure 1).

Using data from repeated hydrographic sections of the DS sill, Mastropole et al. (2017) characterized the different water mass components of the DSO. They showed that Arctic-origin overflow water (referred to here as Arctic Intermediate Water, AIW) is the densest component and is the dominant water mass found in the deep (> 500 m) trough of the section. This water mass is formed during wintertime deep convection in the Greenland and Iceland Seas and is believed to contribute to the DSO via the NIJ (Våge et al., 2011). A recent study argued that AIW found at DS primarily originates from the Greenland Sea gyre (Huang et al., 2020). Recirculating Atlantic Water (RAW) is found above the AIW on the Greenland side of the section, which is advected to Denmark Strait along the east Greenland shelfbreak and slope by the EGC (Rudels et al., 2002). Formation of RAW occurs during atmospheric cooling in the cyclonic boundary current circulation of the Nordic Seas, specifically in the Norwegian Sea, and in the Arctic Ocean (Mauritzen, 1996). In addition, Rudels et al. (2002) argued that the denser water masses are overlain by a stratified, low salinity lid, which also descends into the Atlantic and contributes to the DSO. This fresh lid was observed in hydrographic sections at DS and to the south of DS (Rudels et al., 2002). This water was also observed in the thermocline of the EGC at Fram Strait and is thought to originate in the Arctic Ocean (Rudels et al., 2002).

The volume transport of the DSO exhibits some interannual variability, with higher transports in 1999-2000 and lower transports between 2001 and 2003 (Dickson et al., 2008; Macrander et al., 2005), but has remained approximately constant between 1995 and 2015 on multi-

annual timescales (Jochumsen et al., 2017). Nevertheless, the properties of the DSO

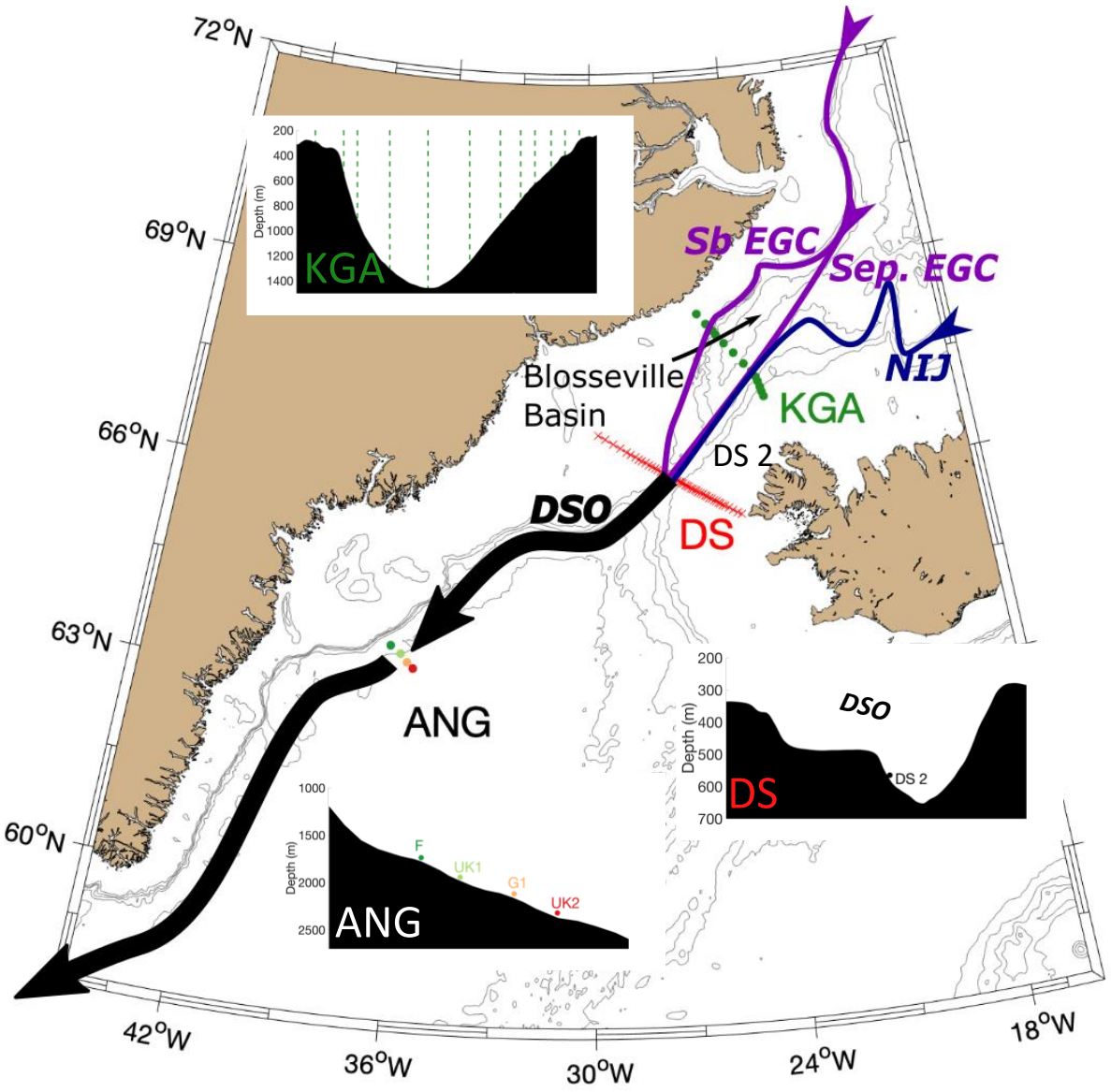

Figure 1. Schematic map of the sources and pathway of the DSO east of Greenland, as well as the location of moorings and the hydrographic section at Denmark Strait (DS). The acronyms are: Separated East Greenland Current (Sep. EGC), Shelfbreak East Greenland Current (Sb EGC), North Icelandic Jet (NIJ), Denmark Strait Overflow (DSO), Kögur array (KGA), Angmagssalik array (ANG). The filled circles indicate the location of mooring data used in this study: DS 2 at DS and F, UK1, G1 and UK2 at ANG. At DS, there is a mooring and a repeat hydrographic section. The inset panels are schematic cross sections of the arrays, with the curved lines indicating the upper boundary of the DSO. The 500 m, 750 m, 1000 m, 1400 m and 2000 m isobaths are shown, which are derived from the IBCAO bathymetry product.

vary on seasonal, interannual and multidecadal timescales (Dickson et al., 2008). In particular, sustained negative salinity and temperature anomalies on intra-annual timescales (i.e. multi-month) have been reported (Dickson et al., 2008; Hall et al., 2011; Jochumsen et al., 2015; Yashayaev & Dickson, 2008). The property variability of the DSO on this timescale is thought to reflect variations in the contributions of its source water masses (Hall et al., 2011; Jochumsen et al., 2015). In this paper, we analyze the hydrographic variability of

DSO source water north of DS, and establish its relationship with property variability of the DSO at the DS and downstream.

It has been frequently argued that wind forcing exerts an important influence on the ocean circulation around Denmark Strait, and that this could have implications for DSO variability. Firstly, the potential role of barrier winds has been identified: these are strong northeasterly winds that occur around Denmark Strait, caused by the high mountains on the east Greenland coast damming the flow of air and causing an offshore pressure gradient that intensifies the wind speed in the along-coast direction (Harden et al., 2011; Moore & Renfrew, 2005; Petersen et al., 2009). Barrier wind events generally occur in winter, when low pressure systems propagate from the North Atlantic into the Nordic Seas around Denmark Strait, inducing high wind speeds (Harden et al., 2011). They have been demonstrated to force spilling of dense water off the East Greenland Shelf south of Denmark Strait (Harden et al., 2014). Furthermore, using concurrent atmospheric and oceanographic data from the southern Blosseville Basin to the north of DS (Figure 1), Håvik and Våge (2018) demonstrated that barrier winds are associated with negative salinity and density anomalies in the Shelfbreak EGC, and elevated volume transports. This could lead to both a freshening and an increased contribution of the Shelfbreak EGC to the DSO.

Second, the wind stress curl in the Blosseville Basin north of Iceland is believed to dictate the relative contribution of the two EGC branches and the NIJ to the DSO (Harden et al., 2016; Köhl et al., 2007) (Figure 1). These studies argue that there exists an anti-correlation between the contributions of the different branches to the DSO on seasonal (Harden et al., 2016) and interannual (Köhl et al., 2007) timescales. Since the currents advect different water masses, this could result in variability in the properties of the DSO itself.

Previous studies highlight wind forcing at DS and further north as a key driver of DSO salinity variability (Hall et al., 2011; Holfort & Albrecht, 2007). These studies emphasize the strong relationship between remote winds and the salinity of the DSO in the Irminger Basin by presenting signficant correlations at plausible lags. Specifically, they argue that strong along-coast northerly winds at DS (Holfort & Albrecht, 2007) and at 75°N (Hall et al., 2011) enhance the volume transport of the EGC, increasing the contribution of the freshest source water and causing freshening of the DSO downstream 2 and 4.5 months later respectively. However, they were not able to confirm that this oceanographic process causes freshening due to sparsity of available data.

In this study, we investigate the response of the ocean to local wind forcing at the Kögur array (KGA) north of DS, using moored ocean observations, and determine its downstream impact on the DSO in DS and in the Irminger Basin. Thus, we provide new insights into why remote wind forcing controls the salinity of the DSO downstream, by identifying the relevant oceanographic processes.

The paper is organized as follows. In the Section 2, we introduce the oceanographic and atmospheric data used. In Section 3, we characterize sustained freshening events within the DSO using mooring data from the Irminger Basin and DS, and CTD data from DS. In Section 4, we investigate the hydrographic variability of DSO source water using a one year mooring dataset from the southern Blosseville Basin. In Section 5, we examine the relationship between remote wind forcing and the salinity of the DSO. Finally, in Section 6, we present conclusions and outline the implications for the downstream evolution of the overflow.

2 Data

2.1 Angmagssalik array

Deep (≥1500 m) moorings with near-bottom instrumentation were deployed in an array (named the Angmagssalik Array; ANG) on the southeast Greenland slope in the Irminger Basin, around 63.5°N, between 1986 and 2015 (Figure 1). The early measurements, between 1986 and 1990, were analyzed by Dickson and Brown (1994). The moorings were equipped with Rotor Current Meters and, from 1998 onwards, Seabird-Electronics-37 SM MicroCAT (MC) instruments, deployed around 20 m above bottom, with additional instruments occasionally deployed 100-300 m higher in the water column.

Near-bottom salinity measurements from the ANG moorings F, UK1, G1 and UK2 are used in this study (see the cross-slope locations in the inset panel of Figure 1). Note that moorings F1F2 and F2 were deployed at different times in the mid-slope region (around 1600-1800 m), and, since they are separated by just 8-9 km, time series derived from these moorings are amalgamated to a single nominal mooring F for simplicity. There was a continuous presence of at least one near-bottom MC between 1998 and 2015, except for one year (1999-2000). We created a gap-free salinity time series, representative of the DSO at ANG by concatenating data from neighbouring moorings. It is not technically gap-free because there are still gaps from mooring turnaround, but these gaps are short. Data from the mooring UK1 were mainly used for this time series, but in 2001-02 and 2006-07, when UK1 data were not available, data from G1 and UK2 were used instead. This data splicing is justified by the high correlation ($r>0.90$; $p<0.01$) between the salinity time series of the neighboring moorings.

The ANG moorings were deployed to capture the bottom intensified DSO, which is known to flow from DS to Cape Farewell along the Greenland slope (Dickson & Brown, 1994) (Figure 1). The array is downstream of the location where the DSO vigorously entrains lighter water, which is thought to occur within 200 km of DS (Voet & Quadfasel, 2010). Therefore, when the DSO passes through ANG it comprises a variety of different water masses: the water that feeds the DSO from the north and the entrained waters.

The salinity data are derived from conductivity, temperature and pressure measurements from the MCs, which have an initial accuracy of 0.0003 S m^{-1}, 0.002°C and 0.1% of full-scale pressure range respectively, but which are prone to fouling, sediment build up or electrode damage to the conductivity cell. Therefore, the MC data were systematically calibrated using ship-deployed conductivity-temperature-depth (CTD) casts as a reference. The MC conductivity measurements frequently underestimated the true conductivity, relative to the CTD reference. To correct this, an offset value was added to the moored conductivity time series and salinity was recalculated with the adjusted conductivity. The offsets ranged from 0.0007 S m^{-1} to 0.0021 S m^{-1}. Note that the accuracy of the calibrated moored salinity is decreased as a result of the additional uncertainty of the reference salinity measurements. The salinity used in this study is practical salinity, which has no units, for consistency with recent studies of the DSO that also used practical salinity. All mooring salinity time series in this study were smoothed using a 2nd order Butterworth filter with a 20-day low-pass frequency cut-off prior to analysis, to remove tidal, inertial and high-frequency eddy influences on the salinity field (von Appen et al., 2017) and for consistency with previous studies (Fischer et al., 2015; Jochumsen et al., 2015). The resulting salinity time series were not sensitive to the order of the Butterworth filter and only fractionally quantitatively affected by the choice of frequency cut-off.

2.2 Denmark Strait

We use property data from a mooring and shipboard hydrographic sections, with the latter providing a greater spatial coverage of the DSO in order to better understand its hydrographic variability.

2.2.1 DS 2 mooring

Since 1995, there has been a continuous presence of at least one mooring at DS. The two main moorings at DS are named DS 1 (bottom depth: 630 m) and DS 2 (bottom depth: 570 m), deployed in the deep trough (Jochumsen et al., 2012). We choose to use the salinity data from the near-bottom (height: 20 m) MC at DS 2 (see inset panel in Figure 1) for two reasons. Firstly, the DS 2 salinity time series is longer than DS 1, and secondly the salinity variance at DS 2 is greater than at DS 1 (Jochumsen et al., 2015), and therefore more likely to capture the freshening events that are the subject of this study. As explained above, we smooth the time series using a Butterworth filter with a 20-day low-pass frequency cut-off.

2.2.2 DS hydrographic section

There is a repeat hydrographic section at DS, known as the Látrabjarg section, which has been regularly occupied by different research institutions since 1990 (von Appen et al., 2014). The eastern half of the section (extending past the deep trough) is one of many hydrographic sections usually occupied each season by the Marine and Freshwater Research Institute of Iceland (MFRI). The section comprises multiple CTD stations spaced between 6 km and 25 km apart (Mastropole et al., 2017) between the Iceland shelf and Greenland shelf (Figure 1; inset panel).

The CTD data have been interpolated onto an evenly spaced grid, with a horizontal resolution of 2.5 km and a vertical resolution of 10 m, by Mastropole et al. (2017). This gridded dataset was updated by Lin et al. (2020) using CTD sections occupied between 2013 and 2018. Although some velocity measurements were made using an Acoustic Doppler Current Profiler (ADCP), we focus here on the CTD data. The majority of the data were acquired by the Icelandic research vessels, the *Bjarni Sæmundsson* and *Árni Friðriksson* (von Appen et al., 2014), using a Sea-Bird-Electronics 911 CTD with SBE 3 temperature and SBE 4 conductivity sensors, and the salinity data were calibrated using Autosal 8400/8400B measurements of water samples (M. Danielsen. Pers. Comms). The accuracy of the salinity data is estimated to be 0.002 (Lin et al., 2020).

2.3 Kögur array

Twelve tall moorings were deployed at the location of another repeat MFRI hydrographic section – the Kögur section (KGA) – 200 km northeast of the DS section between 2011 and 2012, in the southern Blosseville Basin (Figure 1); see Harden et al. (2016) for details. The moorings were equipped with fixed depth and profiling instruments to measure the properties and velocity of the water. The KGA data are used to investigate the hydrographic variability of DSO source water originating in the north, for example the varying contributions of the EGC and the NIJ (e.g. Harden et al., 2016; Håvik et al., 2017; Rudels et al., 2002; Våge et al., 2013).

All the data were calibrated and processed as per Harden et al. (2016). Briefly, the point hydrographic data were factory calibrated before and after deployment, and the data from the

profiling instruments were calibrated using the point hydrographic measurements as a reference. Unfortunately, the velocity data derived from the 2011-12 and 2012-13 deployments of the upward-looking ADCP on the Greenland shelf (KGA12) were found to be erroneous. We discovered that the flow speeds recorded at KGA12 in 2013-14 are systematically higher than in 2011-13. By extracting the tidal component of flow using UTide (Codiga, 2011), we found the tidal component of flow at KGA12 in 2013-14 to be in close agreement with both a neighboring mooring (KGA14), and output from a barotropic tidal model – AOTIM-5 (Padman and Erofeeva, 2004), see Opher (2021) for details. Vertical cross sections of velocity and properties were constructed using Laplacian-spline interpolation by Harden et al. (2016). The gridded data product has a horizontal, vertical and temporal resolution of 8 km, 50 m and 8 hours respectively. The volume transport values reported in this paper are lower than reported by Harden et al. (2016), because the data associated with the erroneous KGA12 velocity are removed (which includes interpolated velocities between KGA12 and KGA11 on the upper slope where overflow water is found). To be clear, velocity beyond KGA11 is set to NaN (not a number) when calculating transports.

2.4 ERA5

We use wind and sea level pressure data from the European Centre for Medium-range Weather Forecast (ECMWF) fifth-generation atmospheric reanalysis product (ERA5) (Hersbach et al., 2020). We use data from east of Greenland in the subpolar North Atlantic and Nordic Seas during the period that coincides with the oceanographic mooring deployments (1998-2015).

The ERA5 data are developed from the previous reanalysis product (ERA-Interim), which showed good agreement with observations in the region (Harden et al., 2011; Harden et al., 2015). Furthermore, a recent study of the Nordic Seas demonstrated good agreement between ERA5 fields and observations over the open ocean, although with higher errors over the marginal ice zone (Renfrew et al., 2021). Nevertheless, the correspondence in wind speeds between ERA5 and aircraft observations was generally good, with a root mean square error of 1.77 m s^{-1} over open ocean and 2.44 m s^{-1} over the marginal ice zone.

3 The annual salinity cycle of the DSO

Using the multiple time series described above, the objective of this section is to characterize the spatiotemporal salinity variability of the DSO. We begin by characterizing the annual cycle first downstream, at ANG, and then at DS.

3.1 Typical characteristics of the annual cycle

3.1.1 Downstream of Denmark Strait at ANG

Sustained freshening events occur annually at ANG. To identify these events, the periods between the maximum that occurs each October-March and the minimum in the following year (or the same year if the maximum occurs between January and March) are indicated by the grey shaded areas in Figure 2a and b. The freshening intensity (ΔS) is shown for each mooring time series in Figure 2c. No minimum magnitude of ΔS (threshold) was used to define a freshening event, but the differences between freshening events are discussed below.

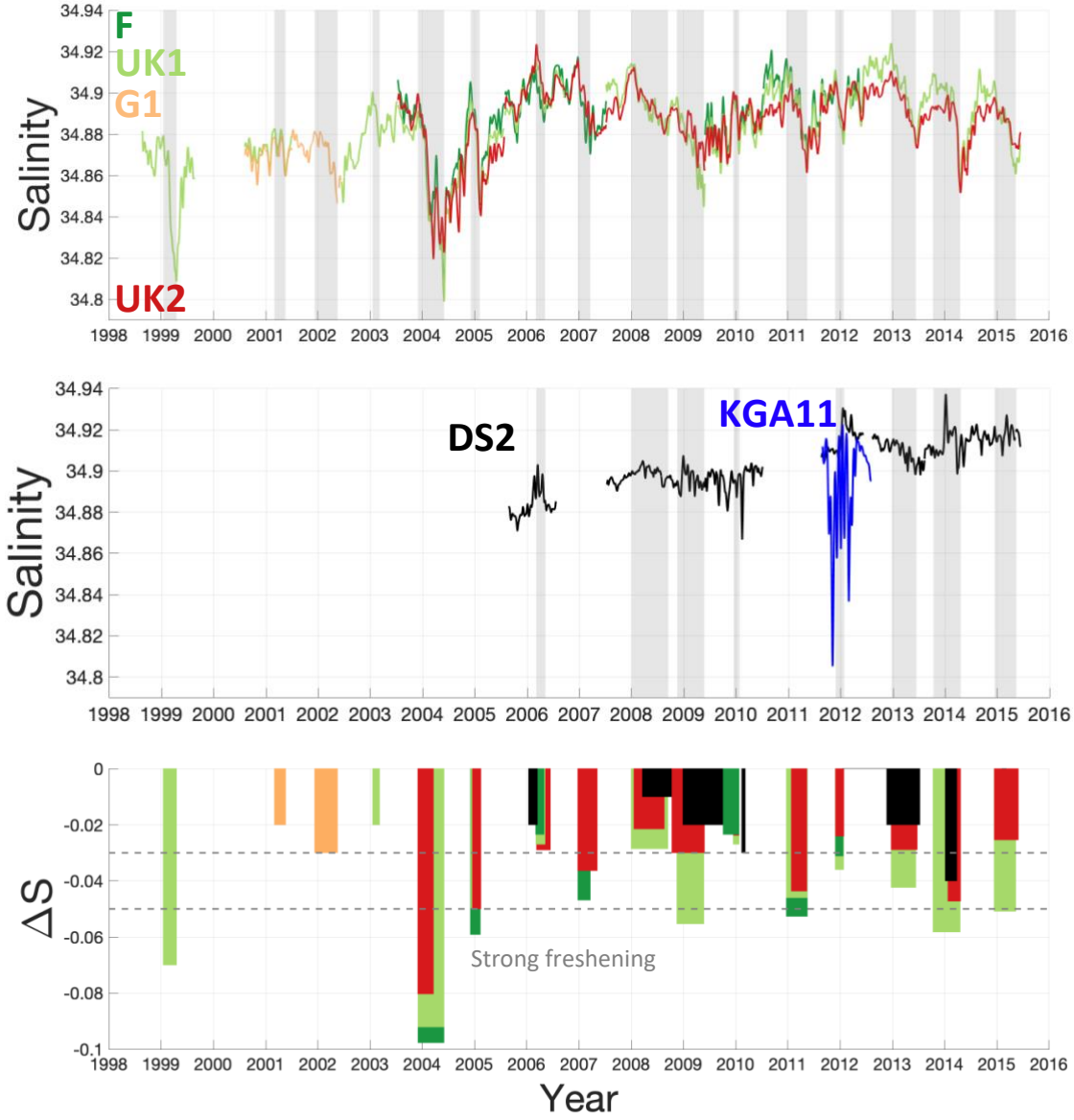

Figure 2. Time series of DSO salinity at (a) ANG, (b) DS 2 and KGA11 and (c) freshening intensity (ΔS) at DS and ANG between 1998 and 2015. The grey shaded areas (in a and b) indicate sustained freshening events at the UK1 mooring. Freshening intensity, or ΔS, is calculated as the difference in salinity between the start and end of the event. The width of the bars represents the duration of the freshening. The different colours represent the different moorings. The year labels mark 1 January each year. Note that freshening intensity is greatest at the shallower moorings at ANG (F and UK1).

Particularly marked freshening ($\Delta S \leq -0.05$) occurs at ANG in 1999, 2003-04, 2004-05, 2008-09, 2010-11, 2013-14 and 2014-15 (Figure 2a and c). Conversely, weak freshening ($\Delta S \geq -0.03$) occurs at ANG in 2001, 2003, 2006, 2008 and 2009-10. The salinity minimum (34.8) of the time series occurs in 2004 at UK1 and F, at the end of the freshening event that year. Note that there is greater freshening at F than UK1 in 2003-04 (Figure 2c) since the salinity at the start of the event at F is higher than at UK1 and the salinity at both moorings is around 34.8 at the end of the event.

Aside from the interannual variation of freshening, identified above, the DSO salinity also varies spatially. The moorings at ANG occupy different density classes of DSO, and thus likely different water mass contributions. The mean potential density ($\boldsymbol{\sigma_\theta}$) at F, UK1 and UK2 is 27.89, 27.91 and 27.94 (all in kg m^{-3}) respectively. While freshening occurs consistently at all three moorings at ANG, the freshening intensity varies across the array (compare length of bars in Figure 2c). Specifically, freshening intensity is greater at the two shallower moorings (F and UK1) than at UK2. The median freshening intensity is -0.05 and -0.04 at F and UK1, respectively, compared with -0.03 at UK2. This implies that the freshening events may originate from lighter density classes of DSO source water.

Note also that the freshening typically occurs in winter and spring, indicating a seasonal salinity cycle. This is confirmed by the fitting of a linear regression model, with a period of one year, to the monthly averaged salinity time series (Figure 3). The time series used for Figure 3 is the concatenated (gap-free) time series (Section 2.1). The annual frequency is associated with a high amount of variance, as evident by a peak in the spectrum (not shown). The salinity maximum of the seasonal cycle occurs in November and the minimum occurs in May, with a peak to trough amplitude of approximately 0.02 (Figure 3). The seasonal cycle represented by the linear regression model explains 37% of the variance of the monthly

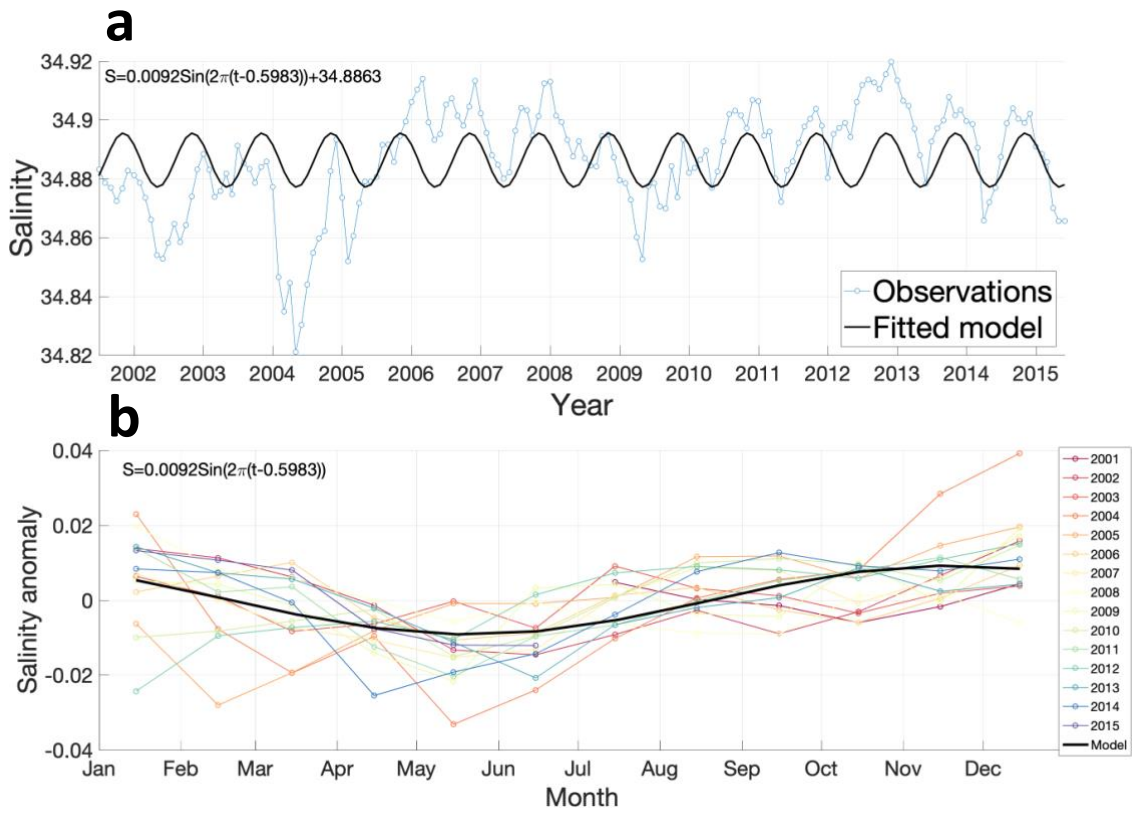

Figure 3. Monthly averaged salinity at ANG. The salinity data are primarily from the UK1 time series, but G1 and F data from 2001-02 and 2006-07 respectively are also used. (a) shows the salinity time series between 2001 and 2015 from mooring observations (blue) and a fitted linear regression model with an annual frequency (black). (b) shows the salinity anomaly (salinity minus annual mean) as a function of calendar month for individual years, from mooring observations (joined up multi-coloured circles) and the mean salinity anomaly of the model with an annual frequency (thick black line). A Fourier transform was carried out on the monthly averaged salinity and the transform was inverted to create the fitted time series with a period of 1 year. The equation for the model is given in black text, where S is salinity and t is time in decimal years.

averaged salinity time series. There was no comparable seasonal signal for temperature (not shown).

3.1.2 At Denmark Strait

The mooring time series at DS used in this study (DS 2) are from the deep trough at DS (Figure 1), where the time-mean density between 2005 and 2015 was 28.02 kg m^{-3} (denser than the densest ANG mooring). The intensity of freshening at DS 2 is either weaker than that observed at ANG, absent, or unknown due to missing data (Figure 2b). For example, while intense freshening occurs at UK1 in 2009 ($\Delta S \sim -0.06$), the freshening intensity at DS 2 is much less (~ -0.02). In fact, the median freshening intensity at DS 2 between 2005 and 2015 is only -0.02, lower than all the ANG moorings, which implies that the freshening does not originate from the denser classes of DSO source water that advect through the trough. Furthermore, entrainment of warm and saline ambient water is known to occur between DS and ANG (Voet & Quadfasel, 2010), which one would expect to weaken any signal passing through the strait.

This difference in salinity variability at the two arrays was demonstrated previously by Jochumsen et al. (2015), who showed that the lagged correlation of salinity between the two locations is not statistically significant. Our results confirm this, using longer concurrent time series. Jochumsen et al. (2015) argued that the salinity variability downstream at ANG must have been caused by variability of entrainment downstream of DS. However, an alternative possibility is that the freshening originates from lighter density classes of DSO that advect through DS above or west of DS 2.

The salinity minimum at ANG generally occurs in May and the maximum in November (Figure 3), indicating that freshening events typically occur between winter and spring. Assuming a 10-20 day transit time between DS and ANG (Jochumsen et al., 2015; Koszalka et al., 2013) – as justified in more detail below – it follows that the salinity minimum (maximum) should typically occur in April/May (November/December) at DS. To investigate this, we analyze the repeat hydrographic section data covering a greater area of the DS. We construct monthly composites from the start and end of the freshening events. Figure 4 shows the mean vertical salinity section and a salinity profile in May and November.

The salinity distribution is largely unchanged between May and November, especially in the denser ($\sigma_\theta > 27.95$ kg m^{-3}) classes of DSO (Figure 4). The salinity profile on the Greenland ledge (i.e. the region where the ocean bottom is flat between the shelfbreak and the trough between 105 km and 130 km in Figure 4b and c) is qualitatively unchanged, with saline dense water overlain by fresher water (Figure 4e). This lower salinity water in the lighter density classes of DSO in both monthly composites is consistent with the description of a fresh lid of the overflow, by Rudels et al. (2002). However, there is a key difference between the months in the properties of the low salinity lid on the ledge which is fresher in May inshore of 120 km (Figure 4b). The difference can also be seen in the salinity difference section (Figure 4d) and the salinity profiles within the 27.76 kg m^{-3} – 27.92 kg m^{-3} density interval (Figure 4e). Similarly, negative DSO salinity anomalies occur in May at ANG, and the freshening is greater in the lighter density classes of DSO downstream. We therefore propose that the negative salinity anomaly within the fresh lid contributes to the sustained seasonal freshening of the DSO each year.

To test whether the fresh lid observed at DS in spring contributes to the freshening of the DSO observed at ANG, we quantify the effect of the fresh lid on the salinity of the overflow.

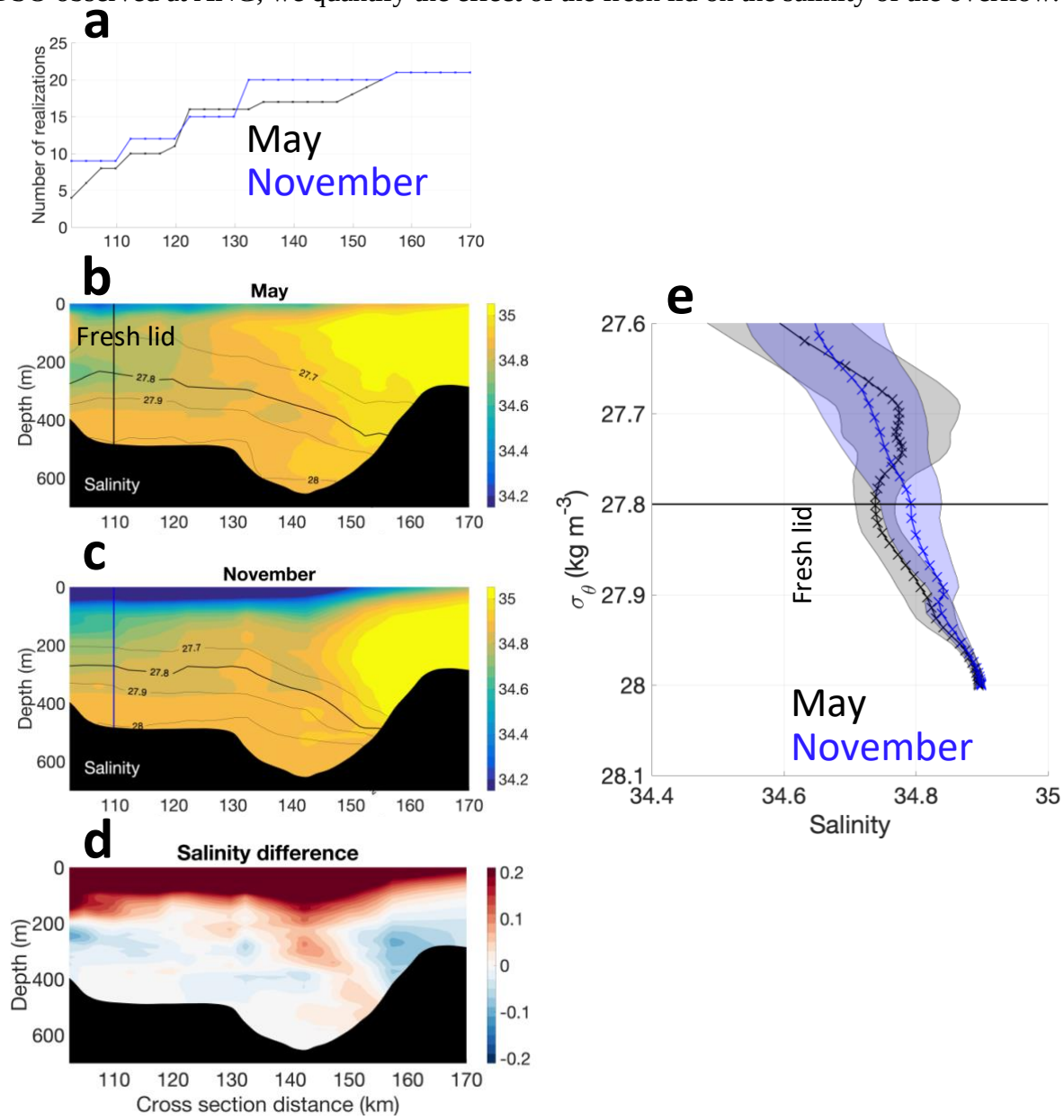

Figure 4. Mean salinity distribution across the Denmark Strait (DS) hydrographic section in May and November using data between 1990 and 2018. (a) shows the number of realizations as a function of cross-stream distance for the two months. (b) and (c) show the mean salinity cross sections in May and November respectively and (d) is the difference between them (May minus November). The black lines are isopycnals (kg m^{-3}), the thick black line is the 27.8 kg m^{-3} isopycnal and the thick vertical lines indicates the location of the profiles shown in (e). (e) Composite salinity profiles versus potential density below the 27.6 kg m^{-3} isopycnal at the location of the vertical lines in (b) and (c) in May and November, respectively. The joined up crosses are the mean and the shaded area represents the mean ± the standard error.

The rationale for this quantification is that the different components of the DSO likely mix between DS and ANG and the water passing through ANG is thus probably a mixture of fresh lid water, RAW, AIW and entrained water (Voet & Quadfasel, 2010). The median DSO water salinity of the mean May section is 0.008 less than the median DSO water salinity of

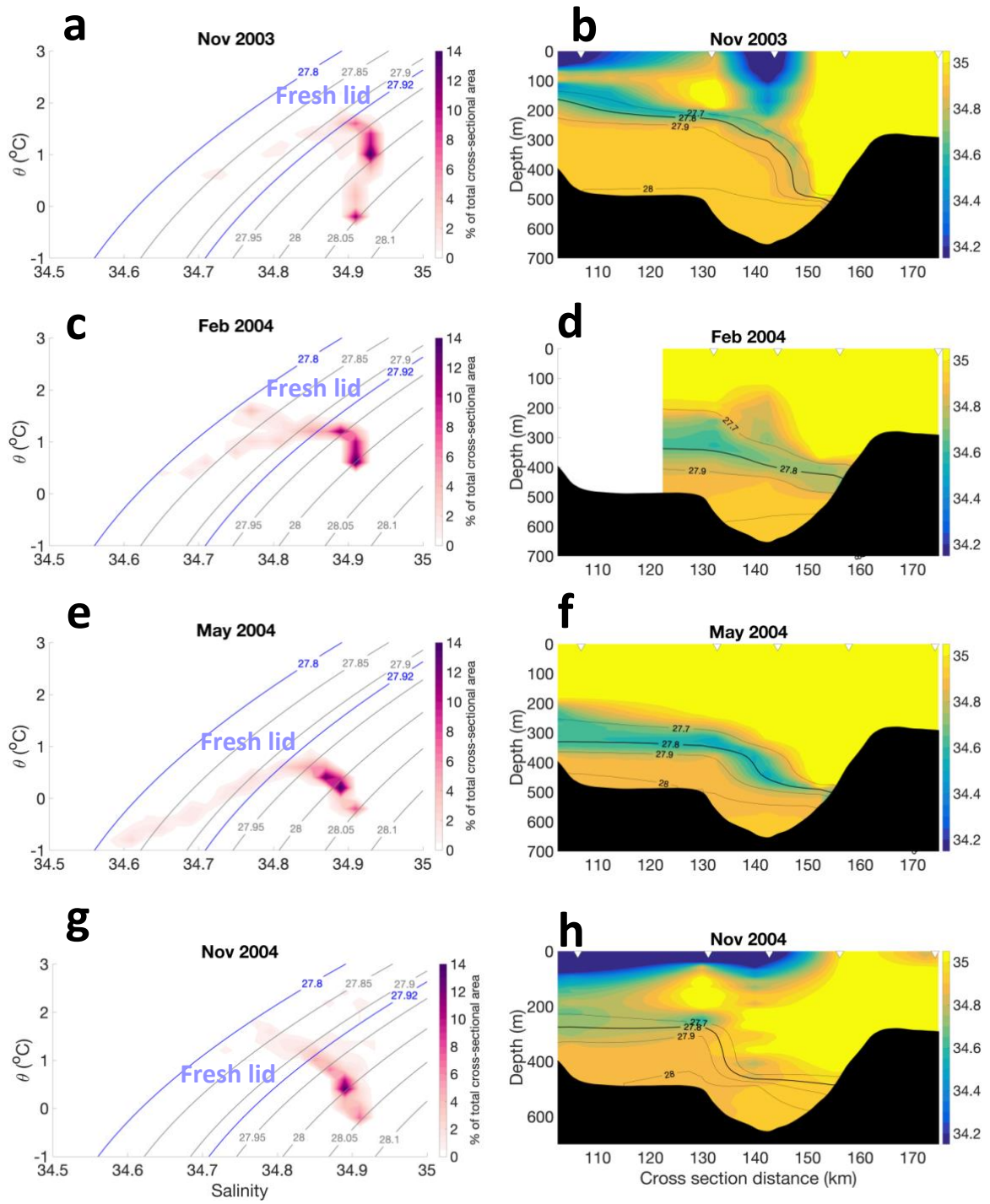

Figure 5. CTD section snapshots of the DS section between 2003 and 2004. The panels in the first column (a,c,e,g) show the θ-S distribution of DSO water (in % of total cross-sectional area) in each θ-S bin. The panels in the second column (b,d,f,h) show the salinity cross-sections.The inverted triangles indicate the location of CTD stations. The black lines are isopycnals (line of constant potential density; in kg m^{-3}). The snapshots occur in November 2003 (a and b), February 2004 (c and d), May 2004 (e and f) and November 2004 (g and h).

the mean November section. This indicates that the property seasonality at DS may plausibly drive the freshening at ANG, since the seasonal change in salinity at the two locations is a similar magnitude. However, a t-test of the two composite sections at DS (May and November; Figure 4b and c) formally finds the difference in DSO salinity is not statistically

significant. This is likely because the seasonal salinity changes are subtle, however we believe that the salinity changes we describe at DS are part of the same annual cycle as we see downstream, at ANG.

3.2 Case study of freshening in 2003-04

To test the idea that the fresh lid drives the annual salinity cycle further, we examine the hydrographic changes in a case study between November 2003 and November 2004 when there was an extreme, prolonged freshening event at ANG (Figure 2). We present one hydrographic section before the event, in November 2003 (Figure 5a and b), two during the event, in February and May (Figure 5c-f), and one after the event, in November 2004 (Figure 5g and h). These snapshots might be influenced by high frequency mesoscale variability; indeed, a bolus (i.e. a thick lens of weakly stratified overflow water, which extends at least 150 m above sill depth) is observed in November 2003, but none are identified in the 2004 sections (Mastropole et al., 2017). An extremely cold and fresh lens is present in February and May 2004 (Figure 5c-f). The core of the fresh lens is a temperature and salinity minima located between 300 m and 500 m depth close to the DSO interface (the $\boldsymbol{\sigma_\theta}$=27.8 kg m^{-3} surface). The fresh lens is associated with the fresh lid of the overflow, which can be best seen in the θ-S curves of February and May 2004 (Figure 5c and e). The occurrence of this anomalous fresh lid coincides with the record salinity minimum at ANG, which occurs in May 2004 (Figure 2a). The lid is characterized by stable salinity stratification and unstable temperature stratification. We define the fresh lid as the water bounded by the 27.8 kg m^{-3} and 27.92 kg m^{-3} isopycnals in the θ-S curves of Figure 5 on the basis of the identification of the fresh lid in the composite (Figure 4e). Note that we use the 27.8 kg m^{-3} isopycnal instead of the 27.76 isopycnal because we are focused on the DSO and thus only show the θ-S distribution of DSO water in Figure 5a, c, e and g.

To test whether the anomalous fresh lid observed at DS in February and May 2004 might cause the freshening of the DSO observed at ANG, we quantify the effect of the fresh lid on the salinity of the overflow as was done previously. At its minimum in May 2004, the median salinity of the DSO at DS is 0.05 lower than in November 2003 and 0.02 lower than in November 2004. This salinity reduction of 0.05 (between November 2003 and May 2004) is roughly half of the freshening intensity of the DSO seen at ANG in that year (Figure 2c), which varied from -0.08 at UK2 to -0.1 at F. Given that the CTD snapshots will not have captured the full extent of the freshening event, we surmise that this freshening is of the right magnitude to explain the downstream freshening.

4 Advection of salinity anomalies from the Shelfbreak EGC to the DSO

4.1 Advection of salinity anomalies

Here, we evaluate the concept that freshening of the Shelfbreak EGC north of DS contributes to freshening of the DSO via advection. The reason we focus on the Shelfbreak EGC is that Håvik and Våge (2018) showed that local Ekman downwelling favorable winds can cause negative salinity anomalies within the Shelfbreak EGC on the upper Greenland slope of the Blosseville Basin, at KGA. We propose that these negative salinity anomalies in the Shelfbreak EGC are transferred into the DSO. We emphasise that our investigation is based on just one year of data, and the level to which these data are representative of other years

cannot be established.

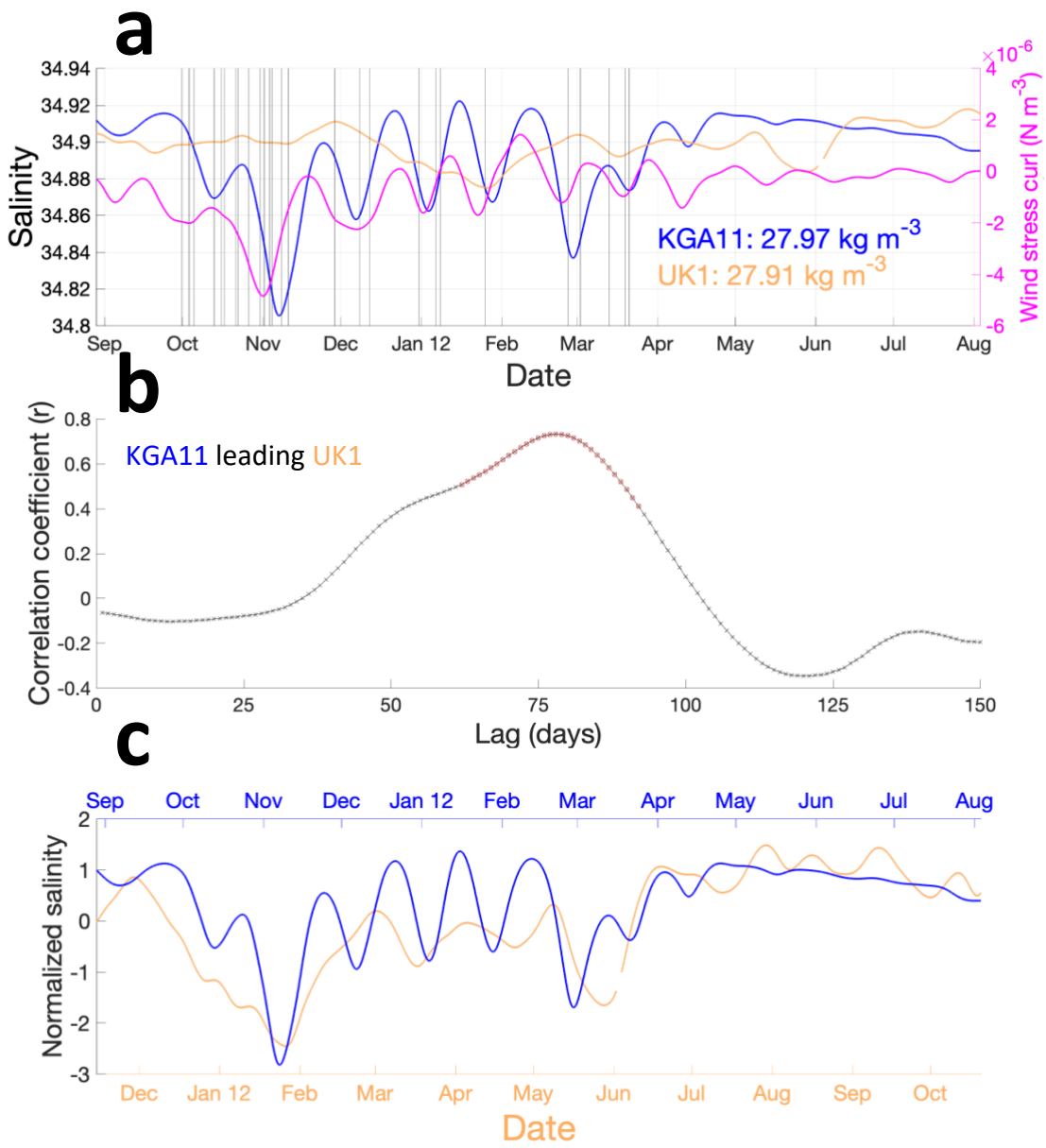

Figure 6. Salinity time series at KGA and ANG in 2011-12 and the lagged correlation between the time series. (a) Time series from the near-bottom MC instrument on the upper Greenland slope mooring (KGA11) and UK1 at ANG. The wind stress curl time series locally at KGA11 is also shown in magenta. The black vertical lines indicate the occurrence of local barrier wind events during the KGA11 deployment, as identified using the procedure introduced by Harden et al. (2011). The time-mean potential density of the two time series is also displayed in panel a. Panel b shows the correlation coefficient against lag time for the UK1 time series lagging the KGA11 time series. Red circles indicate statistically significant correlations at the 95% level. Panel c shows the time series normalized (mean removed and divided by their standard deviations) with the x axis of the KGA11 time series shifted by 78 days to compare the time series at the lag of maximum correlation.

We compute the correlation between the Shelfbreak EGC salinity in the Blosseville Basin and the salinity of the DSO in the Irminger Basin (Figure 6). To represent the Shelfbreak EGC, we use the salinity time series from the near-bottom MC at KGA11 (bottom depth: 550 m, instrument height above bottom: 5 m; see location on map in Figure 7). This time series is

also shown in Figure 2b for comparison with the downstream salinity time series. To represent the DSO, we use the salinity time series from UK1. Both time series were smoothed using a 2nd order 20 day low-pass Butterworth filter (Section 2.1), and the reduced number of degrees of freedom caused by the smoothing was accounted for in the calculation of statistical significance of the correlations. Note the greater high frequency variability at KGA11 than at UK1 (Figure 6a), which might be caused by processes affecting the near surface part of the water column (depth < 1000 m), such as mesoscale eddies (de Steur et al., 2017) or perhaps buoyancy loss at the ocean surface driving overturning.

We find that freshening at KGA11 is reflected 2-3 months later downstream, at ANG (Figure 6a). Freshening events occur at KGA11 in early November 2011 and February/March 2012, when the salinity falls below 34.84. Meanwhile, at ANG, freshening events occur in January 2012 and late May 2012, around 2-3 months after the freshening events at KGA. This may indicate the advection of anomalies between moorings. However, the advection of salinity anomalies between the two moorings is also affected by changes in ocean circulation, for example changes in the volume transport of the Shelfbreak EGC.

In November 2011, a large anticyclonic eddy moved southward through KGA, driving enhanced southward volume transport of the Separated EGC and northward volume transport of the Shelfbreak EGC, as described by de Steur et al. (2017). This eddy event is probably not related to the freshening of the Shelfbreak EGC in early November (Figure 6a) because the centre of the eddy passed through the array between 14 November and 19 November (de Steur et al., 2017), at least 7 days after the salinity minimum in the Shelfbreak EGC on 7 November. The southward volume transport of the Shelfbreak EGC was generally weak during early November (Harden et al., 2016) and this will likely increase the transit times between the moorings.

High, statistically significant ($p<0.01$), lagged correlations (up to $r=0.73$) occur between the time series at KGA and ANG (Figure 6b). The lag time of maximum correlation is 78 days, which is close to the transit time estimate based on measured advection speeds and known advection pathways (Figure 7; justified below). The correlation at this time lag is illustrated in Figure 6c, which shows normalized time series with the KGA11 time series shifted forward by 78 days.

To estimate this transit time, the advection pathway is divided into two legs: between KGA and DS, and between DS and ANG (Figure 7). In the first leg, the advection distance is calculated by integrating along the 500 m isobath on the upper Greenland slope from KGA to DS, which approximates the pathway of the Shelfbreak EGC. The bathymetry data are from the General Bathymetric Chart of the Oceans (GEBCO_2014) grid (Arndt et al., 2013). While an advection speed of 0.08 m s^{-1} is based on the mean along-stream flow speed at KGA11 (bottom depth of 550 m). The reason we use this time series is because the instrument in question is located within the core of the Shelfbreak EGC (in the time-mean sense) within the DSO source water ($\sigma_\theta > 27.8$ kg m^{-3}; see Harden et al., 2016). This yields a transit time from KGA to DS of 43 days. For the second leg, from DS to ANG, we assume that the freshening signal is advected by the DSO, and use an estimate from Koszalka et al. (2013) of approximately 20 days. Therefore, the total estimated transit time from KGA to ANG is of order 60 days (Figure 7). This is slightly shorter than the lag time of maximum correlation between salinity of the moorings (78 days), which implies that the pathway of salinity signals in the Shelfbreak EGC may perhaps recirculate, as a result of dynamics such as the anti-cyclonic eddy in November 2011 described by de Steur et al. (2017), delaying transit times as a result.

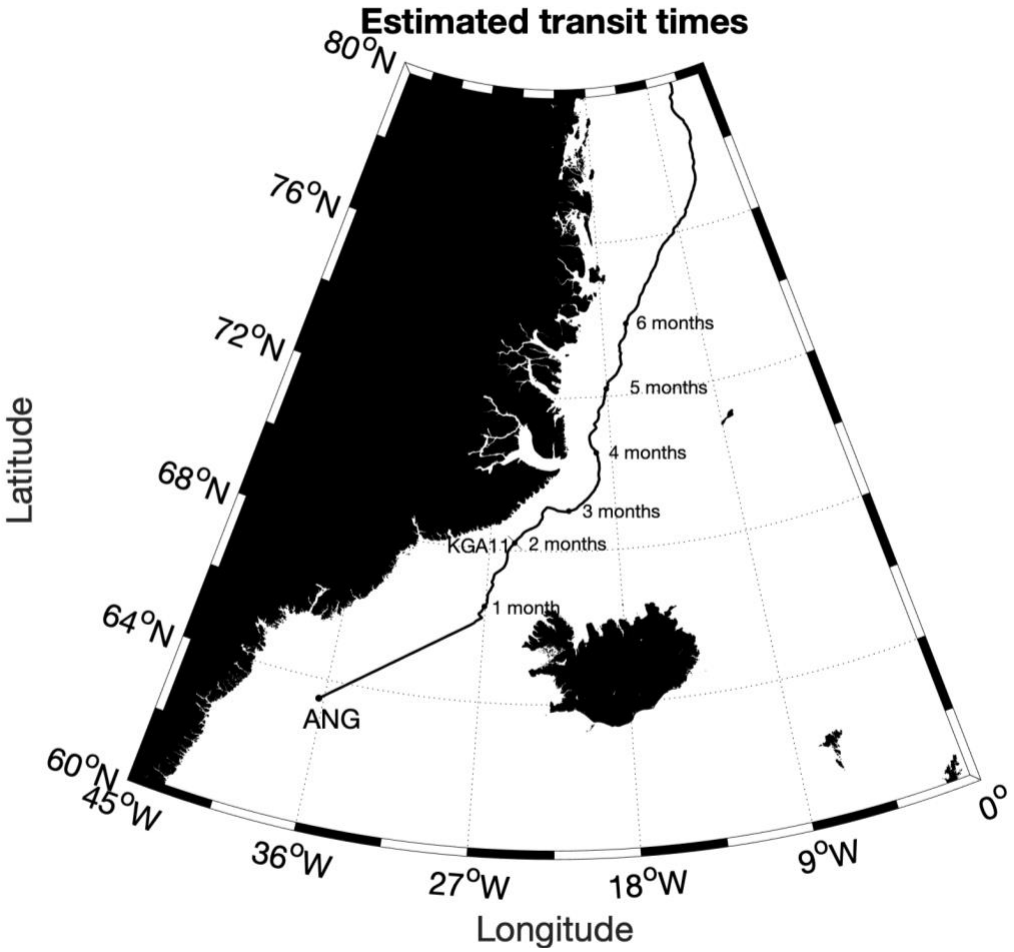

Figure 7. Estimated transit times of freshening signals from the Shelfbreak EGC to the DSO at ANG. The transit times are estimated by dividing the along-isobath distance (advection distance) by the time mean velocity at 550 m at KGA11 in 2011-12 (advection time). The bathymetry used is the GEBCO_2014 grid (Arndt et al., 2013).

The estimated transit time suggests that the lag time of maximum correlation in salinity between moorings is physically plausible. Furthermore, the reduction in density of the DSO between KGA11 (27.97 kg m^{-3}), and UK1 (27.91 kg m^{-3}), can plausibly be explained by modification by the entrainment of lighter water (Dickson et al., 2008 ; Voet & Quadfasel, 2010). Therefore, we conclude that wintertime freshening of the Shelfbreak EGC likely contributes to freshening of the DSO.

4.2 Causes of Shelfbreak EGC freshening

The barrier wind events occurring in 2011-12 locally to KGA11 were identified using the methodology presented by Harden et al. (2011), and are marked as black lines on Figure 6a. Periods of frequent barrier wind events are associated with freshening on the upper Greenland slope. For example, there were 15 barrier wind events between 30 September 2011 and 10 November 2011, which are associated with freshening and culminated in the salinity minimum of 34.80 on 7 November 2011. After this barrier wind events were less frequent

and salinity minima not as low, while from April onwards there were no barrier wind events and no pronounced salinity minima.

This pattern of freshening during barrier wind events might be explained by the compensation of near-surface onshore Ekman transport by offshore transport at depth, which injects the fresh water on the shelf into the core of the Shelfbreak EGC (Håvik & Våge, 2018). Alternatively, the November salinity minimum might be explained by Ekman pumping causing isopycnal heaving, associated with the strong negative wind stress curl recorded for three weeks between mid-October and early-November (Figure 6a; see also de Steur et al., 2017). The most negative wind stress curl occurred in early November, which coincides almost exactly with the salinity minimum at KGA11. This negative wind stress curl event is unconnected to the large anti-cyclonic eddy described by de Steur et al. (2017).

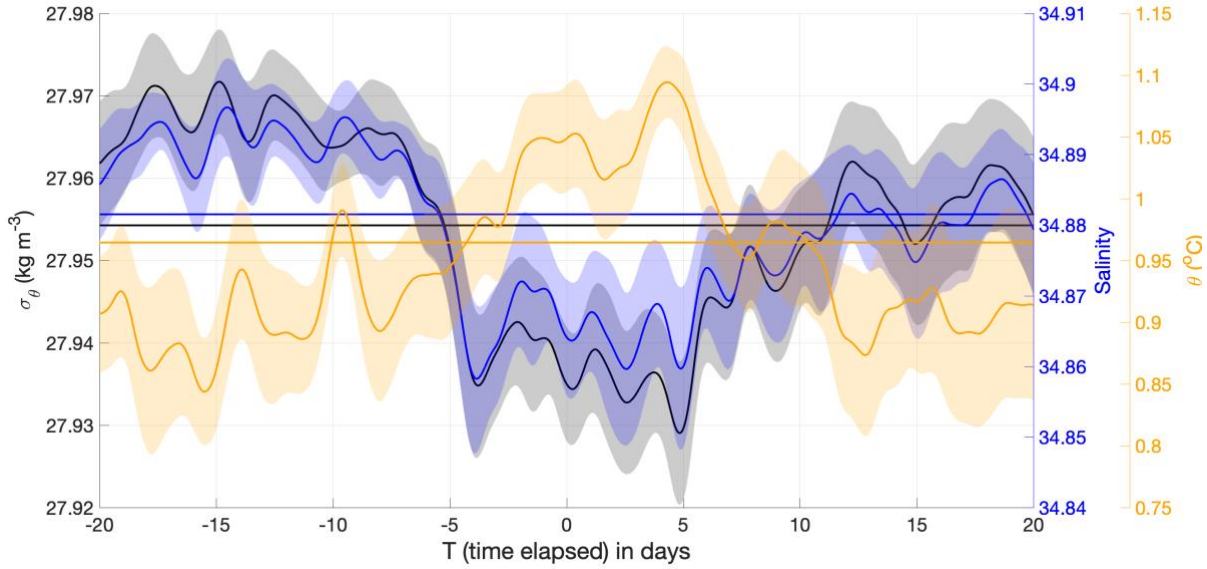

Figure 8. Composite response of ocean properties on the upper Greenland slope to barrier wind events in winter 2011-12. Salinity (blue), potential temperature (orange) and potential density (black) are shown. The data used are from the near-bottom MC at KGA11 (Figure 6). The composite was calculated by averaging the properties during 27 barrier wind events, where T=0 is the time of barrier wind occurrence, T<0 is before the barrier wind event and T>0 is after the event. The horizontal lines show the winter mean properties. The thick time series lines are the composite mean and the shaded area represents the standard error.

There appears to be a close correspondence between the salinity and the local wind stress curl, with the wind stress curl leading the salinity (Figure 6a). However, note that the pronounced freshening event, in February/March, is not associated with strong negative wind stress curl (Figure 6a), showing that other processes can drive local freshening.

By constructing a composite response of the ocean to the barrier wind events, we find that barrier winds are associated with freshening on the upper Greenland slope (Figure 8). There were 27 barrier wind events in 2011-12 and the mean salinity between 20 days before (T=-20 days) and 20 days after (T=20 days) for all events was calculated to construct the composite. Note that many barrier wind events overlap and it is not always possible to distinguish individual events, but by using the composite we seek to guage the typical impact of barrier winds. The broad response is a warming/freshening extending from several days before the peak winds to roughly a week after (Figure 8). The reason for warming and freshening before the barrier wind event in the composite may be that barrier winds tend to last for a few days

and occur in quick succession (see black vertical lines in Figure 6a) and therefore the period immediately before and after T=0 in the composite also captures barrier wind forcing. The property changes are indicative of a deepening of water masses, since the water overlying the near-bottom MC is warmer and fresher (Harden et al., 2016). This reinforces the assertion of Håvik and Våge (2018) that downwelling favourable winds drive negative salinity anomalies on the upper Greenland slope north of DS. Note that this is similar to the barrier wind forcing seen by Harden et al. (2014), which causes spilling of fresh, but dense, water off the shelf to the south of DS.

The property changes associated with barrier winds may imply that vertical mixing occurs within the Shelfbreak EGC, with fresh lid water introduced at greater depths than usual. One mixing process that may take place is shear-driven vertical turbulent mixing, brought about by wind-driven Ekman downwelling causing the isopycnals over the Greenland upper slope to steepen. After the barrier winds, we conjecture that the fresh lid water remains at greater depths downstream and thus approaches the DS sill deeper than usual. Conversely, we reject the idea that the water masses are just temporarily redistributed by barrier winds before returning to their original depth, because this does not account for vertical mixing that likely takes place during barrier winds. The greater depth of the fresh anomaly makes the fresher water more likely to be entrained into the main plume of the overflow around DS, as opposed to entering the Greenland shelf where it may be modified by Irminger Water found there (Mastropole et al., 2017) and become more saline, before cascading off the shelfbreak to join the DSO. The more direct route for the fresh source water of the DSO when the fresh anomaly approaches deeper in the water column may give rise to the winter-spring freshening of the current.

5. Denmark Strait Overflow salinity driven by remote wind forcing

We argue above that wind forcing (both barrier winds and wind stress curl) drives hydrographic variability of DSO source water north of DS, consistent with previous studies (Hall et al., 2011; Harden et al., 2016; Holfort & Albrecht, 2007; Köhl et al., 2007). This variability has previously been outlined as a key driver of DSO salinity variability in the Irminger Basin by Holfort and Albrecht (2007) and Hall et al. (2011). However, it remains unclear where the wind forcing exerts the greatest influence on the DSO, with previous studies (Hall et al. 2011; Holfort & Albrecht, 2007) having reached different conclusions. We now aim to reconcile previous disagreements on the role of remote winds on DSO salinity.

We calculate lagged correlation between the wind and the DSO salinity in the Irminger Sea, using the monthly averaged ERA5 wind fields and monthly averaged moored salinity data from ANG (Figure 9). The salinity time series used for Figure 9 is the concatenated gap-free time series (Section 2.1) The mean and trend was removed from the salinity time series. We used the northward component of wind at, and to the north of, 70ºN and the northeastward component of wind to the south of this latitude. The justification for using these two wind components rather than scalar wind speed or only zonal and meridional components is that the leading theory to explain wind driven freshening of the DSO is Ekman downwelling (Section 4.2), which is driven by winds parallel to the coast, i.e. northerly winds north of around 70ºN and northeasterly winds south of 70ºN. The aim of this investigation is to determine whether remote wind forcing may be driving the annual salinity cycle of the DSO.

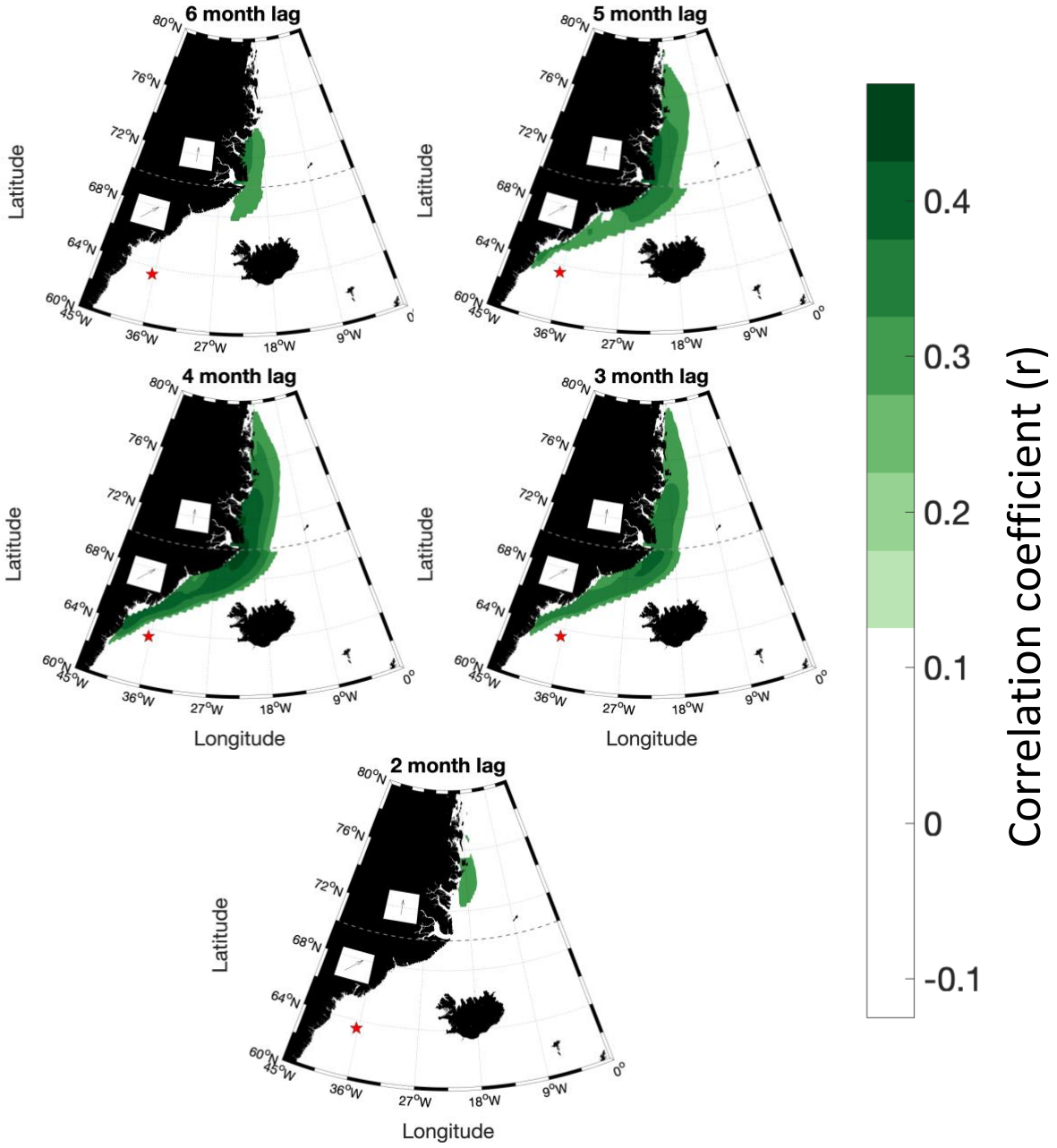

560 *Figure 9. Lagged correlations between the component of wind in a given direction and the salinity of the DSO at ANG (location marked by red star). The northward component of the wind at, and to the north of, 70ºN (dashed line) and the the northeastward component of wind south of this latitude are used for the correlation calculation. The correlations vary from a lag of 2 to 6 months (wind leading salinity). The colors indicate the magnitude of the correlation coefficient (r). Only those correlations which are significant at the 95% level are shown.*

561
562 Therefore, the common practice of removing the seasonality from time series prior to
563 calculating correlations is not carried out. As a result we attach an important caveat to the
564 correlations presented below, which may of course arise through chance and do not
565 necessarily imply a causal relationship. However, we show later that we believe there is a
566 causal relationship between wind and salinity of the overflow.

567 Correlations of r>0.375 occur between the wind over the Greenland continental margin at
568 64ºN-74ºN and the DSO salinity at a 4 month lag (Figure 9), with maximum correlation

(r>0.425) at around 70ºN. The correlations at the 4 month lag are higher than at any other time lag. Correlations of r>0.375 also occur in a small area at around 69ºN at a 3 month lag, with maximum correlation (r=0.41) at 69.25ºN 23.25ºW. Low correlations also occur over the Greenland continental margin to the north of 68ºN at 5-6 month lag. At a 2 month lag, low correlations (r>0.225) are found in a small area to the north of 70ºN. However, this isolated area of correlation may not imply a physical link with the overflow salinity, and could instead occur because of the auto-correlation of the wind time series and the fact that there is a causal link between the wind and overflow salinity at a 3 month lag. Conversely, this may indicate the occasionally faster advection times arising from wind forcing of the Shelfbreak EGC in some years. Alternatively, this could indicate that wind driven Coastal Trapped Waves, such as the high frequency waves that have a phase speed of 0.38 m s^{-1} (Gelderloos et al., 2021), may influence the salinity of the overflow too. Note that at a 1 month lag and zero lag, no correlation is found between the wind and salinity of the DSO.

The correlations have a plausible physical interpretation, namely that the wind forcing is leading to local freshening which is then advected to the ANG mooring, via the Shelfbreak EGC and DSO. The lag times of maximum correlation are consistent with the estimated transit times (compare Figure 9 with the estimated transit times in Figure 7). The estimated transit time from 70ºN to ANG is four months and from 69ºN to ANG is three months, providing evidence for a causal relationship between the wind and the salinity of the DSO.

6. Discussion

In this section we characterize and investigate the variability of the different sources of the DSO. In particular, we analyze the differing properties of the water masses advected by the Shelfbreak EGC, the Separated EGC and the NIJ using hydrographic mooring data from KGA, deployed in the Blosseville Basin 200 km upstream of DS, from 2011-12.

6.1 Characteristics of DSO source water

The freshest source water of the DSO is found in the pycnocline of the Shelfbreak and Separated EGC branches. Figure 10 shows the time-mean velocity section at KGA, with the two EGC branches and the NIJ labeled. The θ-S characteristics of the three currents are shown in Figure 11. The Shelfbreak and Separated EGC are surface-intensified currents found on the Greenland shelfbreak and lower Iceland slope, respectively (Figure 10). By contrast, the NIJ is a mid-depth intensified current found over the mid/upper Iceland slope. Visualised as a time-average, the Separated EGC and NIJ are merged, but the two are physically separate at individual times (Harden et al., 2016; Huang et al., 2019). These three branches are the main conduits of DSO source water. This was demonstrated by Harden et al. (2016), who showed that the mean net southward volume transport of DSO source water through KGA in 2011-12 is 3.5 Sv, similar to the time-mean volume transport of the DSO though DS, which is 3.2 Sv (Jochumsen et al., 2017).

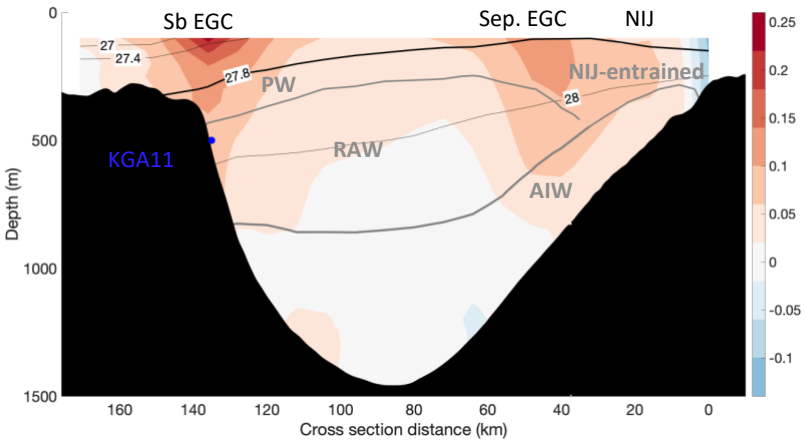

606

Figure 10. Time-mean along-stream velocity (m s^{-1}; positive=southwestward) at KGA in the Blosseville Basin, in 2011-12. The acronyms are Shelfbreak EGC (Sb EGC), Separated EGC (Sep. EGC), North Icelandic Jet (NIJ), Polar Water (PW), Recirculating Atlantic Water (RAW), and Arctic Intermediate Water (AIW). The filled blue circle indicates the location of the MC instrument at KGA11, from which the salinity time series is used. The black lines are isopycnals (in kg m^{-3}), with the thick black line indicating the upper boundary of DSO source water, and the thick grey lines indicating the average location of the RAW and AIW boundaries, as identified using the θ - S definitions from the literature (see text).

607

608 Previous studies (e.g. Harden et al., 2016; Våge et al., 2011) have argued that the main dense
609 water masses advected by the currents are the AIW ($\theta < 0$°C) and the RAW ($\theta > 0$°C, S >
610 34.90), whose locations are labeled in Figure 10. The RAW is primarily transported by the
611 EGC branches, while the AIW is primarily transported by the NIJ (Harden et al., 2016; Våge
612 et al., 2011; Våge et al., 2013).

613 The water overlying the dense water masses is relatively fresh pycnocline water, which is
614 termed Polar Water for the EGC branches and NIJ-entrained for the NIJ (Figure 11) for
615 reasons outlined below. Water denser than 27.8 kg m^{-3} is traditionally thought to contribute to
616 the volume transport of the DSO (Dickson & Brown, 1994). There is some DSO source water
617 denser than 27.8 kg m^{-3} found outside of the traditional water mass boundaries established by
618 previous studies. The DSO source water overlying the RAW in the EGC branches includes a
619 very fresh component (Figure 11), stratified by salinity rather than temperature, indicating a
620 contribution from polar origin water, i.e. water originating from the Arctic Ocean;
621 accordingly this water is termed PW. In comparison, the DSO source water overlying the
622 AIW in the NIJ is relatively saline (Figure 11) and is stratified by both temperature and
623 salinity. This water is likely ambient water entrained into the NIJ between the Iceland Sea
624 and KGA (Semper et al., 2019) and is thus termed NIJ-entrained.

625 Since the freshest DSO source water derives from fresh PW overlying the RAW in the
626 Shelfbreak EGC and Separated EGC, increased volume transport of the EGC branches is a
627 likely candidate for driving freshening events; this is explored in the next section.

628 **6.2 Alternative mechanism of DSO freshening**

629 The barrier winds that result in the freshening of the shelfbreak EGC also enhance the
630 strength of the current. We now seek to gauge the impact of this, and other processes that
631 change the strength of the upstream source water pathways, on the downstream DSO. The

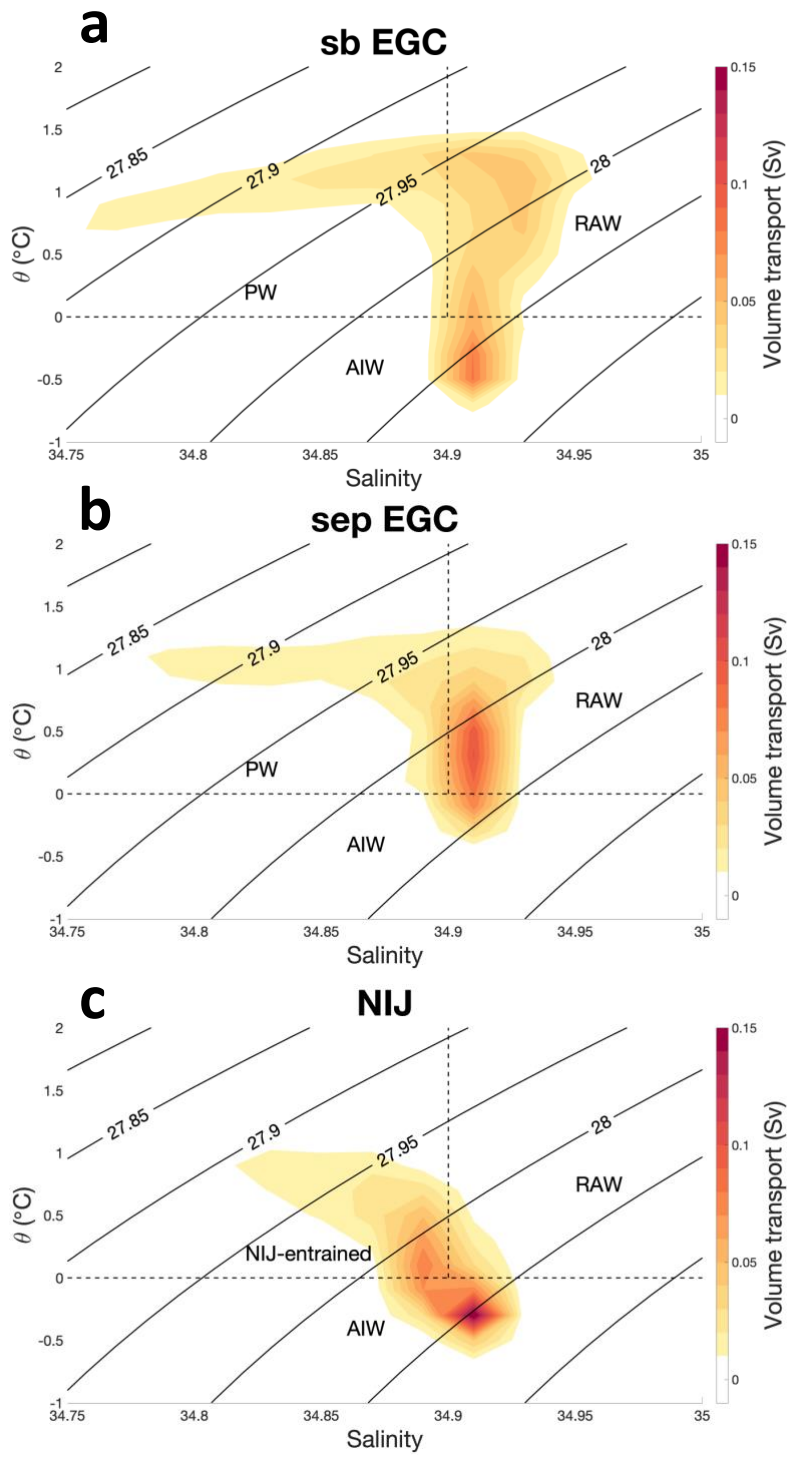

632

Figure 11. Time-mean volume transport (shading) plotted in θ-S space for the three main currents which contribute to the DSO – the Shelfbreak EGC (sb EGC), Separated EGC (sep EGC) and North Icelandic Jet (NIJ) using KGA data from 2011-12. The bins have dimensions of 0.02 by 0.2ºC. The volume transport is in Sv (1 Sv = 10^6 m^3 s^{-1}), with positive values indicating southwestward transport. The horizontal boundaries of the currents are identified using the end-member algorithm of Harden et al. (2016). The temperature and salinity range of the water masses, established in previous studies, are shown by the dashed black lines, with Recirculating Atlantic Water (RAW), Arctic Intermediate Water (AIW), Polar Water (PW) and NIJ-entrained water labelled. The NIJ-entrained refers to the component of the NIJ which is warmer than 0ºC and assumed to be entrained into the current. The black lines are isopycnals (in kg m^{-3}).

633

approach is to use the transport-weighted salinity. The rationale for using the transport-weighted salinity in this study is the assumption that the different components of DSO mix south of DS (Voet & Quadfasel, 2010). This has been used previously to investigate the salinity transformation of the Mediterranean Outflow (Baringer & Price, 1997) and the salinity variability of water masses in the Florida Straits (Szuts & Meinen, 2017). We propose that, should the volume transport of the EGC branches (which carry fresher DSO source water than the NIJ) be enhanced, and the volume transport of the NIJ be decreased, the transport weighted salinity would decrease, indicating a net freshening of the DSO source water. Conversely, when the volume transport of the EGC branches is lower, and the volume transport of the NIJ higher, the transport weighted salinity would increase. Or, to express it another way, the ratio of the volume transport of the EGC branches to the NIJ should control the variability of the transport weighted salinity.

To assess a single salinity value downstream, the upstream transport weighted salinity is used, which accounts for both the salinity and the volume transport of the different source water branches of the DSO passing through KGA. The transport-weighted salinity ($\bar{\mathbf{S}}$) equation used is adapted from (Baringer & Price, 1997):

$$\overline{S} = \frac{\int_{H=0}^{H=\eta} \int_{x=x1}^{x=x2} S \cdot v \, dx \, dz}{\int_{H=0}^{H=\eta} \int_{x=x1}^{x=x2} v \, dx \, dz}$$

where S is the salinity, *v* is the along-stream velocity (positive=southwestward), *x1* and *x2* are the lateral boundaries of the DSO, *H* is the height above the bottom and η is the height of the DSO interface. In contrast to Section 4 when a single MC was used, here we use the gridded KGA data of Harden et al. (2016) which covers a greater extent of the DSO source water.

The time series of the volume transport of the DSO source waters, via the EGC branches and the NIJ, and $\bar{\mathbf{S}}$ are shown in Figure 12. As first shown by Harden et al. (2016), the branches tend to compensate each other seasonally, with high combined EGC transports in winter, when the NIJ is weak, and low combined EGC transports in summer, when the NIJ is stronger. When the EGC branches are strong, the volume transport of PW (i.e. the fresh pycnocline water overlying the RAW) is enhanced. Therefore, $\bar{\mathbf{S}}$ is freshest in winter and more saline in the other seasons (Figure 12). Specifically, $\bar{\mathbf{S}}$ is lowest (34.85) in January and late February/early March. The mean winter (December-January-February) $\bar{\mathbf{S}}$ is 34.867, compared with 34.882 in summer and autumn months (June-November). The difference in seasons is 0.015, which is similar to the seasonality in salinity of the DSO (0.02) observed at ANG between 1998 and 2015 (Figure 3). This reflects the fact that when the southward volume transport of the combined EGC increases in winter, the supply of PW to the DSO increases, likely driving the seasonal freshening of the DSO downstream at ANG.

Assuming that the southward volume transport of the EGC through KGA is elevated in winter in most years, the argument that this mechanism contributes to the annual salinity cycle of the DSO is strengthened. Harden et al. (2016) reasoned that the hydrographic seasonality observed in 2011-12 is representative of other years. Specifically, they argued that the ocean circulation in the Blosseville Basin is largely governed by local wind stress curl forcing, which changes from positive in the winter to negative in the summer. This supports the early idea of Köhl et al. (2007), who proposed that the volume transport of DSO

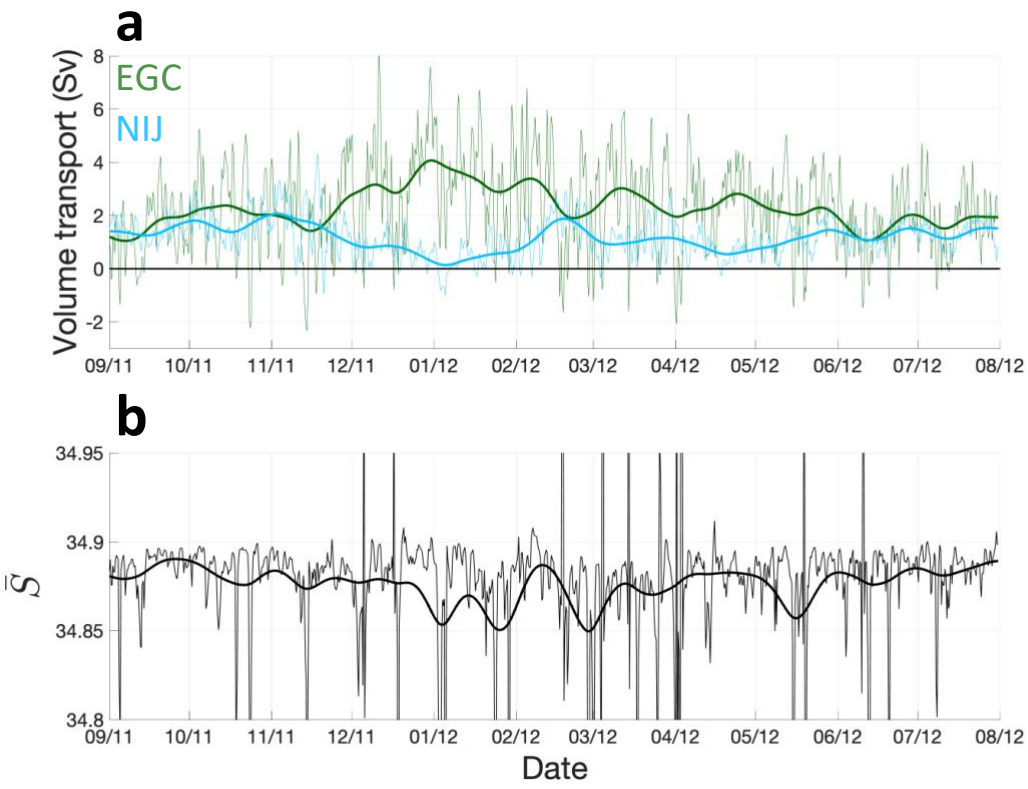

Figure 12. Time series of (a) volume transport of DSO source water via the combined EGC (green) and the NIJ (blue), and (b) transport weighted salinity ($\bar{S}$) at KGA in 2011-12. The volume transport time series are based on the 8 hourly gridded dataset of Harden et al. (2016). The thick lines are smoothed with a Butterworth filter with a 20-day low pass frequency cut-off.

source water via the EGC is anti-correlated with the volume transport of DSO source water via the NIJ leading to a relatively steady supply of dense water to the DSO.

While we argue that the salinity variability of the overflow is dictated by salinity changes of the Shelfbreak EGC in Section 4, here we show that the changes in volume transport of the different source water branches cannot be ruled out as a cause of salinity variability downstream. We are not able to state the relative importance of changes in salinity versus changes in volume transport with a single year of upstream mooring data. However, it seems likely that both mechanisms contribute to the salinity variability of the overflow.

7 Conclusions

We have identified, for the first time, a consistent annual salinity cycle of the DSO. We find no evidence of a corresponding annual temperature cycle. Freshening of the DSO is seasonal and caused by both the wintertime freshening and the increase in equatorward volume transport of the Shelfbreak EGC in the Blosseville Basin, 200 km north of DS. The winter-spring freshening of the DSO is intensified in lighter density classes on the Greenland side of the overflow. This freshening signal has been missed previously by mooring observations in the deep trough of DS, whose near-bottom hydrographic sensors predominantly monitor a single water mass – AIW. These moorings do not appear to capture the variability of lighter DSO water masses, such as the water masses advected by the EGC. While the high variability of properties at the deep moorings on short timescales (daily and weekly; see for example

Spall et al. 2019) indicate the occasional presence of other water masses at Denmark Strait (Macrander et al. 2007), we believe that for longer timescales (seasonal and multiannual) the DS 1 and DS 2 moorings primarily capture variability in AIW. It could be a priority for future observational campaigns to monitor DSO variability using shallower moorings occupying lighter components of the DSO. However, we appreciate that this is logistically challenging due to the fishing activity and very strong currents, and may not be possible at present. In light of these observational difficulties, the continued use of ocean circulation models to understand the contribution of different sources to the overflow (e.g. Koszalka et al. 2013), the mixing of overflow with other water masses (e.g. Koszalka et al. 2017) and the drivers of high frequency variability at Denmark Strait (e.g. Gelderloos et al. 2021) is vital for future progress.

Furthermore, we link this freshening of the DSO to the presence of low salinity lids at DS, previously described by Rudels et al. (2002), which exhibit clear seasonality in their properties. Freshening of the low salinity lids may arise when the southward volume transport of fresh, polar origin water within the EGC increases, or when the Shelfbreak EGC is freshened during barrier wind events. Specifically, the salinity of the Shelfbreak EGC 200 km north of DS is correlated with the overflow salinity at a lag time of around 3 months, which is consistent with estimated transit times. However, this is based on just one year of concurrent mooring data and further years of contemporaneous salinity time series, both north and south of the sill, are required to corroborate this finding.

We also showed that there is a strong relationship between the northerly/northeasterly remote wind forcing over the length of the east Greenland shelfbreak and the salinity of the DSO in the Irminger Basin. The two variables are significantly correlated, with wind leading overflow salinity by 2-6 months. The location of the correlation moves south with shorter lag times, between a 6 month lag and 3 month lag, indicating an input of wind driven variability all along the coast between 80ºN and 64ºN. Maximum correlations occur at a 4 month lag for the wind at 70ºN and the overflow salinity in the Irminger Basin. This lag time is consistent with estimated advection times. The physical interpretation of this correlation is plausible, and demonstrates that the wind forced salinity variability of the Shelfbreak EGC likely influences the property variability of the DSO downstream.

Yashayaev and Dickson (2008) demonstrated that negative salinity and temperature anomalies are advected by the DSO along the southeast Greenland slope and into the Labrador Sea. The anomalies were observed in the deep (>3000 m) center of the Labrador Sea one year after being observed at the ANG moorings (Yashayaev & Dickson, 2008). This shows that there is a direct connection between the wind stress forcing north of Denmark Strait (which drives the freshening events) and the property variability in the deep Labrador Sea on a 1-1.5 year timescale. The advection of property anomalies downstream from DS and ANG may be investigated in conjunction with observations from the Overturning in the Subpolar North Atlantic Programme (OSNAP) array (at 57ºN) to better understand the interaction of different dense water masses that contribute to the deep limb of the AMOC (i.e. DSO water, Iceland-Scotland Overflow Water and Labrador Sea Water).

Data availability statement

The data which supports this study are available from various locations. The gridded Denmark Strait hydrographic dataset used for characterizing salinity seasonality and the Kögur mooring data used for investigating salinity anomalies are available on the Woods Hole Oceanographic Institute Kögur website (kogur.whoi.edu). The DS 2 mooring salinity

time series used for characterizing salinity seasonality are available at Pangaea, via (insert url/doi when available) and the salinity time series from the four Angmagssalik moorings, also used for characterizing salinity seasonality are available at the Cefas datahub, via (insert url/doi when available). The ERA5 reanalysis output can be accessed from the Copernicus Climate Change Service (C3S) Climate Data Store (https://cds.climate.copernicus.eu/#!/search?text=ERA5&type=dataset).

Acknowledgments

Firstly, we are indebted to all those that helped to collect, process and quality control the data from the Angmagssalik array, the Látrabjarg section and the Kögur array. We thank Kerstin Jochumsen for providing access to the Denmark Strait mooring data. We also thank those involved in preparing the gridded Denmark Strait hydrographic section dataset. Many thanks to Peigen Lin and Kerstin Jochumsen for providing us with the extra CTD data from the Látrabjarg section. The authors thank the two anonymous reviewers whose comments/suggestions helped improve and clarify this manuscript. This paper contains modified Copernicus Climate Change Service information (2020). This research was funded by: NERC EnvEast DTP studentship NE/L002582 (JO) and Cefas Seedcorn DP371 (JO, SRD); as well as by NERC, by AFIS (NE/N009754/1) (IR), JAB is funded by NE/L011166/1, ORCHESTRA (NE/N018095/1) and ENCORE (NE/V013254/1) and RP is funded by the US National Science Foundation grants OCE-1756361 and OCE-1558742. Cefas work on the Angmagssallik array was supported by multiple international partners including NSF, NOAA-CORC-ARCHES, WHOI-OCCI, European Community's 5th & 7th framework programme under grants ASOF-W (contract EVK2-CT-2002-00149) & No. GA212643 (THOR: "Thermohaline Overturning – at Risk", 2008-2012) and from UK Department for Environment, Food and Rural Affairs (DEFRA) including A1222, SD0440 & ME5102. Our work is dedicated to the memory of Bob Dickson.

References

Arndt, J. E., Schenke, H. W., Jakobsson, M., Nitsche, F. O., Buys, G., Goleby, B., ... & Wigley, R. (2013). The International Bathymetric Chart of the Southern Ocean (IBCSO) Version 1.0—A new bathymetric compilation covering circum-Antarctic waters. *Geophysical Research Letters*, *40*(12), 3111-3117. https://doi.org/10.1002/grl.50413

Baringer, M. O. & Price, J. F. (1997). Mixing and spreading of the mediterranean outflow. *Journal of Physical Oceanography*, *27*(8), 1654–1677. https://doi.org/10.1175/1520-0485(1997)027<1654:MASOTM>2.0.CO;2

Codiga, D. L. (2011). Unified tidal analysis and prediction using the utide matlab functions. Technical Report 2011-01. Graduate School of Oceanography, University of Rhode Island, Narragansett, RI. 59pp.

de Steur, L., Pickart, R.S., Macrander, A., Våge, K., Harden, B., Jónsson, S., et al. (2017). Liquid freshwater transport estimates from the East Greenland Current based on continuous measurements north of Denmark Strait. *Journal of Geophysical Research: Oceans*, *122*(1), 93-109. https://doi.org/10.1002/2016JC012106

Dickson, R. R., & Brown, J. (1994). The production of North Atlantic Deep Water: Sources, rates, and pathways. *J. Geophys. Res.*, *99*(C6), 12,319–12,341. https://doi.org/10.1029/94JC00530

Dickson, B., Dye, S., Jónsson, S., Köhl, A., Macrander, A., Marnela, M., et al. (2008). The overflow flux west of Iceland: variability, origins and forcing. In Arctic–Subarctic Ocean Fluxes, 443–474. Springer. Dordrecht.

Gelderloos, R., Haine, T. W., & Almansi, M. (2021). Coastal trapped waves and other subinertial variability along the Southeast Greenland coast in a realistic numerical simulation. *Journal of Physical Oceanography*, *51*(3), 861-877. https://doi.org/10.1175/JPO-D-20-0239.1

Hall, S., Dye, S., Heywood, K., & Wadley, M. (2011). Wind forcing of salinity anomalies in the Denmark Strait Overflow. *Ocean Science*, *7*(6), 821–834. https://doi.org/10.5194/os-7-821-2011

Harden, B. E., Pickart, R. S., & Renfrew, I. A., (2014). Offshore transport of dense water from the East Greenland shelf. *J. Phys. Oceanogr.*, **44**, 229–245. https://doi.org/10.1175/JPO-D-12-0218.1

Harden, B. E., Pickart, R. S., Valdimarsson, H., Våge, K., de Steur, L., Richards, C., et al. (2016). Upstream sources of the Denmark Strait Overflow: Observations from a high-resolution mooring array. *Deep Sea Research Part I: Oceanographic Research Papers*, *112*, 94–112. https://doi.org/10.1016/j.dsr.2016.02.007

Harden, B. E., Renfrew, I. A., & Petersen, G. N. (2011). A climatology of wintertime barrier winds off southeast Greenland. *Journal of Climate*, *24*(17), 4701–4717. https://doi.org/10.1175/2011JCLI4113.1

Harden, B. E., Renfrew, I. A. & Petersen, G. N., (2015). Meteorological buoy observations from the central Iceland Sea, *J. Geophysical Research - Atmospheres*, **120,** 3199–3208. https://doi.org/10.1002/2014JD022584

Håvik, L. & Våge, K. (2018). Wind-driven coastal upwelling and downwelling in the shelfbreak East Greenland Current. *Journal of Geophysical Research: Oceans*, *123*(9), 6106–6115. https://doi.org/10.1029/2018JC014273

Håvik, L., Våge, K., Pickart, R. S., Harden, B., Appen, W. J. V., Jónsson, S., & Østerhus, S. (2017). Structure and variability of the shelfbreak East Greenland Current north of Denmark Strait. *Journal of Physical Oceanography*, *47*(10), 2631-2646. https://doi.org/10.1175/JPO-D-17-0062.1

Hersbach, H., Bell, B., Berrisford, P., Hirahara, S., Horányi, A., Muñoz-Sabater, J., ... & Thépaut, J. N. (2020). The ERA5 global reanalysis. *Quarterly Journal of the Royal Meteorological Society*, *146*(730), 1999-2049. https://doi.org/10.1002/qj.3803

Holfort, J. & Albrecht, T. (2007). Atmospheric forcing of salinity in the overflow of Denmark Strait. *Ocean Science*, *3*(3), 411–416. https://doi.org/10.5194/os-3-411-2007

Huang, J., Pickart, R. S., Huang, R. X., Lin, P., Brakstad, A., & Xu, F. (2020). Sources and upstream pathways of the densest overflow water in the Nordic Seas. *Nature communications*, *11(1)*, 1-9. https://doi.org/10.1038/s41467-020-19050-y

Huang, J., Pickart, R.S., Valdimarsson, H., Lin, P., Spall M.A., & Xu, F. (2019). Structure and Variability of the North Icelandic Jet from two years of mooring data. *Journal of Geophysical Research, 124*(6), 3987-4002. https://doi.org/10.1029/2019JC015134

Jochumsen, K., Köllner, M., Quadfasel, D., Dye, S., Rudels, B., & Valdimarsson, H. (2015). On the origin and propagation of Denmark Strait Overflow water anomalies in the Irminger basin. *Journal of Geophysical Research: Oceans*, *120*(3), 1841–1855. https://doi.org/10.1002/2014JC010397

Jochumsen, K., Moritz, M., Nunes, N., Quadfasel, D., Larsen, K. M., Hansen, B., et al. (2017). Revised transport estimates of the Denmark Strait Overflow. *Journal of Geophysical Research: Oceans*, *122*(4), 3434-3450. https://doi.org/10.1002/2017JC012803

Jochumsen, K., Quadfasel, D., Valdimarsson, H., & Jónsson, S. (2012). Variability of the Denmark Strait Overflow: Moored time series from 1996–2011. *Journal of Geophysical Research: Oceans*, *117*(C12). https://doi.org/10.1029/2012JC008244

Köhl, A., Käse, R. H., Stammer, D., & Serra, N. (2007). Causes of changes in the Denmark Strait Overflow. *Journal of Physical Oceanography*, *37*(6):1678–1696. https://doi.org/10.1175/JPO3080.1

Koszalka, I. M., Haine, T. W., & Magaldi, M. G. (2013). Fates and travel times of Denmark Strait Overflow water in the Irminger basin. J*ournal of Physical Oceanography*, *43*(12), 2611–2628. https://doi.org/10.1175/JPO-D-13-023.1

Koszalka, I. M., Haine, T. W., & Magaldi, M. G. (2017). Mesoscale mixing of the Denmark Strait Overflow in the Irminger basin. *Ocean Modelling*, *112*, 90-98. https://doi.org/10.1016/j.ocemod.2017.03.001

Lin, P., Pickart, R. S., Jochumsen, K., Moore, G. W. K., Valdimarsson, H., Fristedt, T., & Pratt, L. J. (2020). Kinematic Structure and Dynamics of the Denmark Strait Overflow from Ship-Based Observations. *Journal of physical oceanography*, *50*(11), 3235-3251. https://doi.org/10.1175/JPO-D-20-0095.1

Macrander, A., Käse, R.H., Send, U., Valdimarsson, H. & Jónsson, S. (2007). Spatial and temporal structure of the Denmark Strait Overflow revealed by acoustic observations. *Ocean Dynamics, 57*(2), 75-89. https://doi.org/10.1007/s10236-007-0101-x

Macrander, A., Send, U., Valdimarsson, H., Jónsson, S., & Käse, R. H. (2005). Interannual changes in the overflow from the Nordic Seas into the Atlantic Ocean through Denmark Strait. *Geophysical Research Letters*, *32*(6). https://doi.org/10.1029/2004GL021463

Mastropole, D., Pickart, R. S., Valdimarsson, H., Våge, K., Jochumsen, K., & Girton, J. (2017). On the hydrography of Denmark Strait. *Journal of Geophysical Research: Oceans*, *122*(1), 306–321. https://doi.org/10.1002/2016JC012007

Mauritzen, C. (1996). Production of dense overflow waters feeding the North Atlantic across the Greenland-Scotland Ridge. Part 1: Evidence for a revised circulation scheme. *Deep Sea Research Part I: Oceanographic Research Papers*, *43*(6), 769-806. https://doi.org/10.1016/0967-0637(96)00037-4

Moore, G.W.K. & Renfrew I.A., (2005). Tip jets and barrier winds: A QuikSCAT climatology of high wind speed events around Greenland, *J. Climate*, **18,** 3713-3725.

Opher, J.G. (2021). The wind driven property variability of the Denmark Strait Overflow, (Doctoral dissertation). Retrieved from UEA Digital Repository. (https://ueaeprints.uea.ac.uk/id/eprint/82740/). Norwich, UK: University of East Anglia.

Padman, L., & Erofeeva, S. (2004). A barotropic inverse tidal model for the Arctic Ocean. *Geophysical Research Letters*, **31**(2).

Petersen, G.N., Renfrew I.A. & Moore G.W.K. (2009). An overview of barrier winds off southeastern Greenland during GFDex, *Quarterly J. Royal Meteorol. Soc.*, **135,** 1950-1967.

Renfrew, I.A., Barrell, C., Elvidge, A. D., Brooke, J. K., Duscha, C., King, J. C., et al. (2021). An evaluation of surface meteorology and fluxes over the Iceland and Greenland Seas in ERA5 reanalysis: the impact of sea ice distribution, *Quarterly J. Royal Meteorological Society*, **147,** 691–712. https://doi.org/10.1002/qj.3941

Rudels, B., Fahrbach, E., Meincke, J., Budéus, G., & Eriksson, P. (2002). The East Greenland Current and its contribution to the Denmark Strait Overflow. *ICES Journal of Marine Science*, *59*(6), 1133–1154. https://doi.org/10.1006/jmsc.2002.1284

Semper, S., Våge, K., Pickart, R. S., Valdimarsson, H., Torres, D. J., & Jónsson, S. (2019). The emergence of the North Icelandic Jet and its evolution from northeast Iceland to Denmark Strait. *Journal of Physical Oceanography*, *49*(10), 2499–2521. https://doi.org/10.1175/JPO-D-19-0088.1

Spall, M.A., Pickart, R.S., Lin, P., von Appen, W.J., Mastropole, D., Valdimarsson, H., et al. (2019). Frontogenesis and variability in Denmark Strait and its influence on overflow water. *Journal of Physical Oceanography*, *49*(7), 1889-1904. https://doi.org/10.1175/JPO-D-19-0053.1

Szuts, Z. B. & Meinen, C. S. (2017). Florida current salinity and salinity transport: Mean and decadal changes. *Geophysical Research Letters*, *44*(20), 10–495. https://doi.org/10.1002/2017GL074538

Våge, K., Pickart, R. S., Spall, M. A., Moore, G., Valdimarsson, H., Torres, D. J., et al. (2013). Revised circulation scheme north of the Denmark Strait. *Deep Sea Research Part I: Oceanographic Research Papers*, *79*, 20–39. https://doi.org/10.1016/j.dsr.2013.05.007

Våge, K., Pickart, R. S., Spall, M. A., Valdimarsson, H., Jónsson, S., Torres, D. J., et al. (2011). Significant role of the North Icelandic Jet in the formation of Denmark Strait Overflow water. *Nature geoscience*, *4*(10), 723–727. https://doi.org/10.1038/ngeo1234

Voet, G. & Quadfasel, D. (2010). Entrainment in the Denmark Strait Overflow plume by meso-scale eddies. *Ocean Science*, *6*(1), 301–310. https://doi.org/10.5194/os-6-301-2010

von Appen, W. J., Koszalka, I. M., Pickart, R. S., Haine, T. W., Mastropole, D., Magaldi, M. G., et al. (2014). The East Greenland Spill Jet as an important component of the Atlantic meridional overturning circulation. *Deep Sea Research Part I: Oceanographic Research Papers*, *92*, 75-84. https://doi.org/10.1016/j.dsr.2014.06.002

von Appen, W. J., Mastropole, D., Pickart, R. S., Valdimarsson, H., Jónsson, S., & Girton, J. B. (2017). On the nature of the mesoscale variability in Denmark Strait. *Journal of Physical Oceanography*, *47*(3), 567-582. https://doi.org/10.1175/JPO-D-16-0127.1

Yashayaev, I., & Dickson, B. (2008). Transformation and fate of overflows in the northern North Atlantic. In Arctic–Subarctic ocean fluxes (pp. 505-526). Springer, Dordrecht.